Recent results from H.E.S.S.

Rafał Moderski
Nicolaus Copernicus Astronomical Center

H.E.S.S. - basic data

– **High Energy Stereoscopic System**;
– **five telescopes** 120 m x 120 m area;
– **4x13 m diameter** spherical main mirror f=13 m, 362 circular mirror facets 60 cm diameter, 4 x 107m^2 collecting area, camera: 960 vacuum tube photo-multipliers, field of view ~5°; 1ns sampling;
– **1x28 m diameter** parabolic mirror f=36 m, 614 m^2 area, 875 hexagonal mirror facets 90 cm (flat-to-flat), camera: 2048 photo-multipliers, 1 ns sampling, field of view ~3.2°, 2.8 t
– duty cycle ~1000h/yr (moonless nights required);
– **energy range: ~30GeV - >10TeV**
– **resolution: angular – 0.1°, energetic – 15% @ 1TeV**
– **sensitivity: 1% Crab (5σ, 25h)**

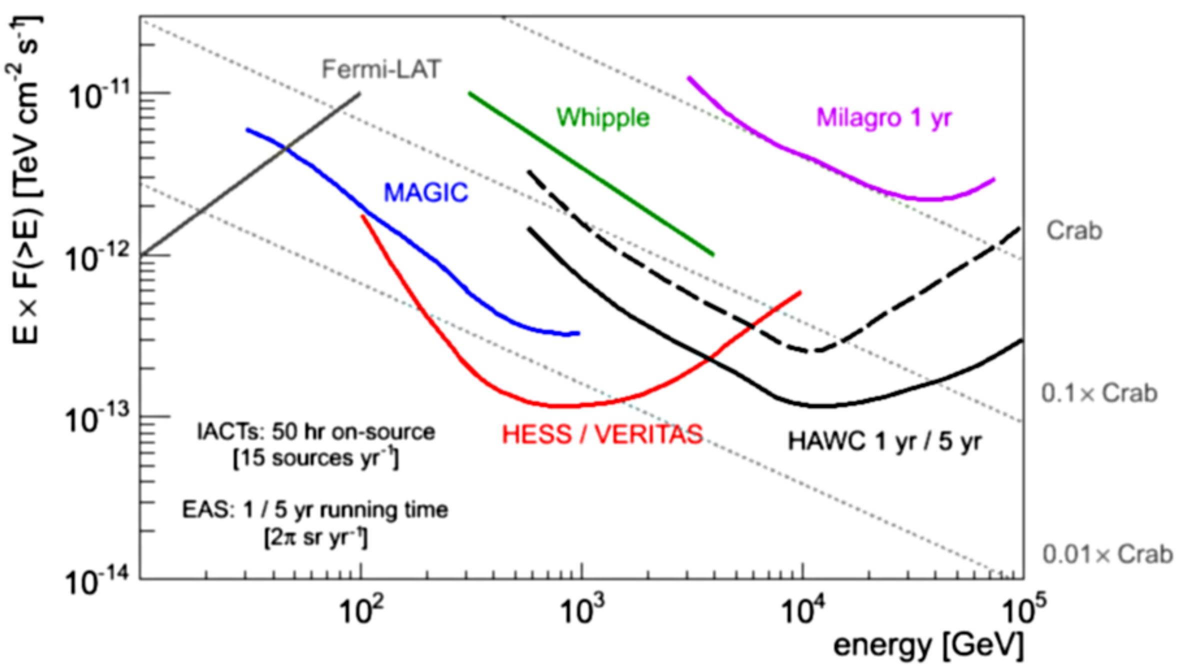

HESS Collaboration

>12 countries, >30 scientific institutions,
>100 scientists

Max-Planck-Institut für Kernphysik, Heidelberg, Germany
Humboldt Universität Berlin, Germany, Institut für Physik
Ruhr-Universität Bochum, Germany, Fakultät für Physik und Astronomie
Universität Erlangen-Nürnberg, Germany, Physikalisches Institut
Universität Hamburg, Germany, II. Institut für Experimentalphysik
Landessternwarte Heidelberg, Germany
Universität Tübingen, Germany, Institut für Astronomie und Astrophysik (IAAT)
Laboratoire Leprince-Ringuet (LLR), Ecole Polytechnique, Palaiseau, France
LPNHE, Universités Paris VI - VII, France,
APC, Paris, France
CEA Saclay, France
Observatoire de Paris-Meudon, DAEC, France
LAPP Annecy, France
Université de Grenoble, France
LPTA, Université Montpellier II, France
CERS, Toulouse, France
Durham University, U.K.
University of Leeds, School of Physics and Astronomy
Dublin Institute for Advanced Studies, Dublin, Ireland

Nicolaus Copernicus Astronomical Center, Polish Academy of Sciences, Warsaw, Poland
J. Dyks, W. Kluźniak, R. Moderski, B. Rudak, A. Zdziarski
Astronomical Observatory, Jagiellonian University, Cracow, Poland
M. Ostrowski, Ł.Stawarz
Institute of Nuclear Physics, Polish Academy of Sciences, Cracow, Poland
J. Niemiec, A. Wierzcholska, S. Cassanova
Astronomical Observatory, University of Warsaw, Poland
T. Bulik
Center for Astronomy, Nicolaus Copernicus University, Toruń, Poland
K. Katarzyński

Charles University, Prag, Czech Republic, Nuclear Center
Yerevan Physics Institute, Yerevan, Armenia
University of Adelaide, Australia, School of Chemistry and Physics
University of Namibia, Windhoek, Namibia
North West University, Republic of South Africa

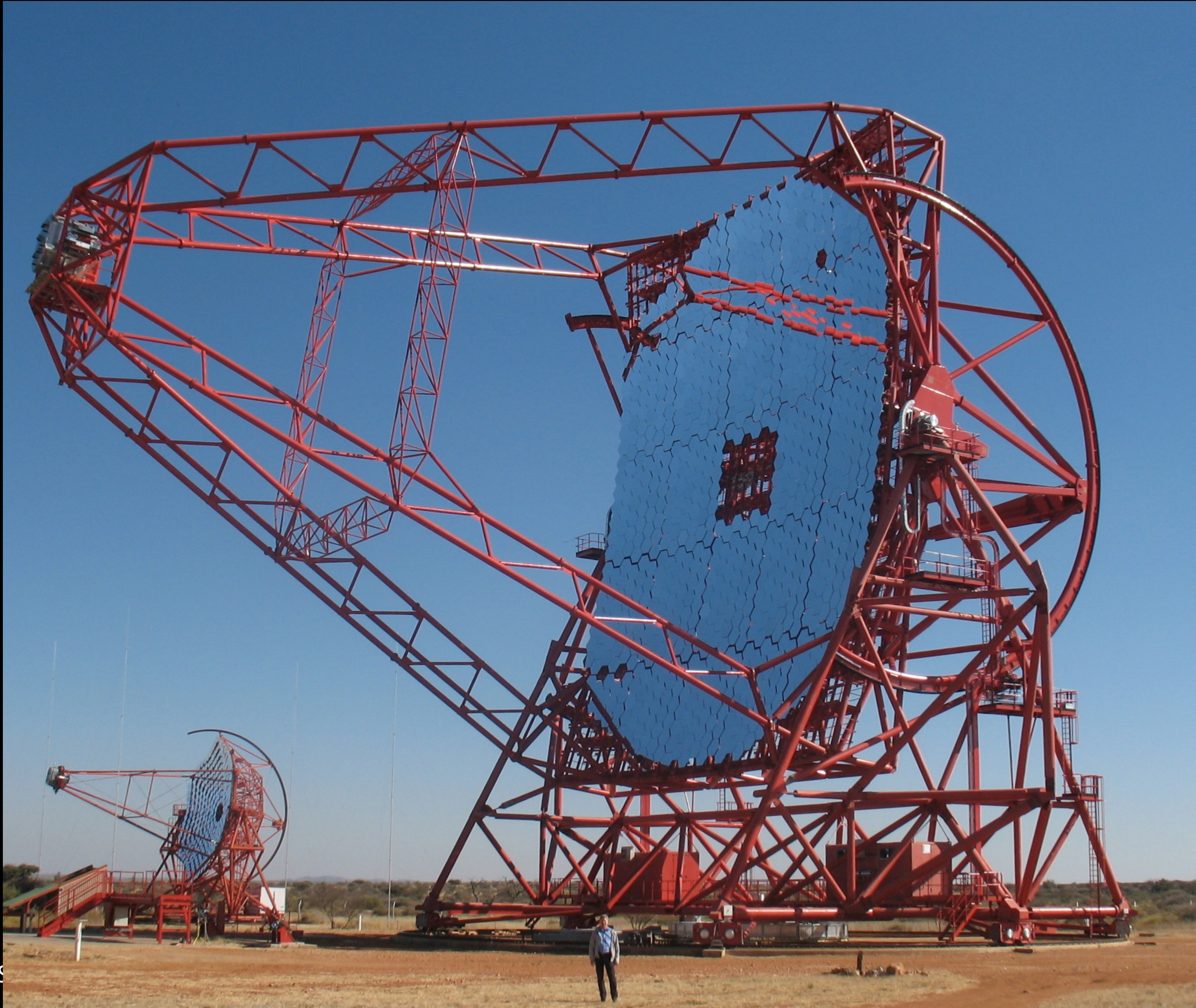

Cherenkov technique

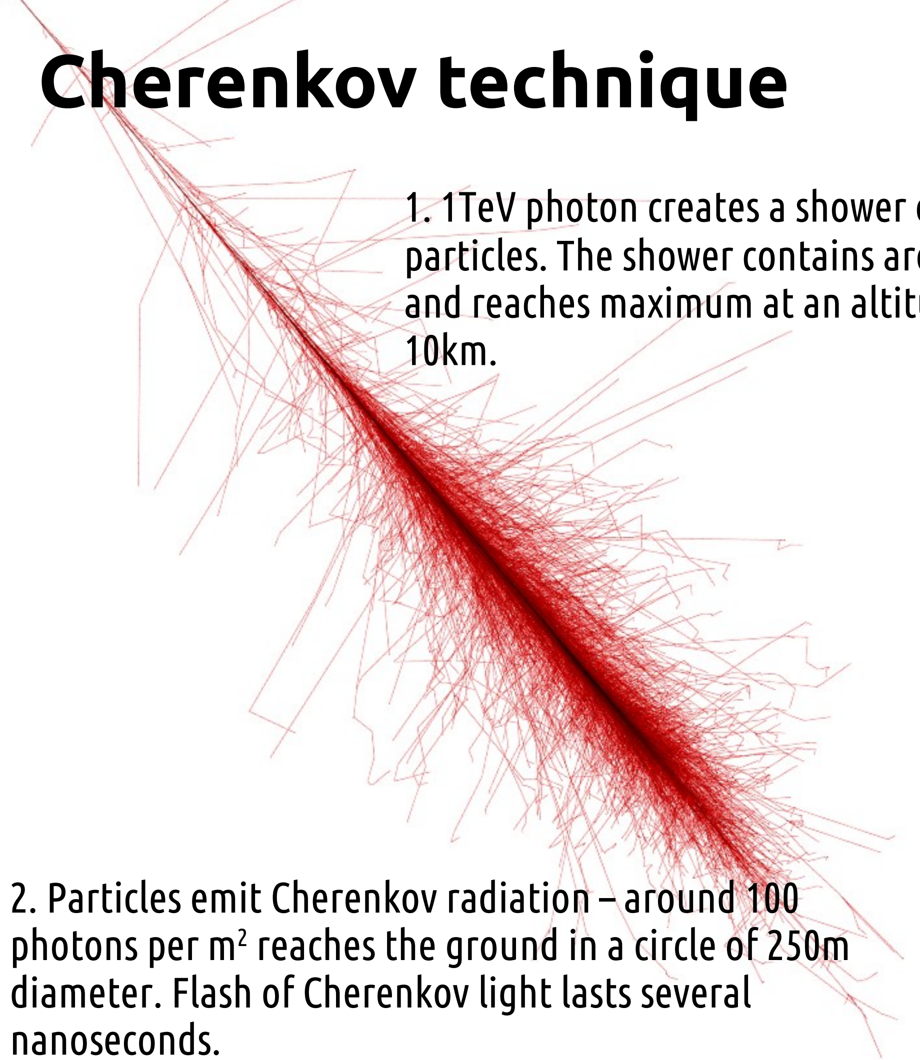

1. 1TeV photon creates a shower of secondary particles. The shower contains around 10^5 e^+e^- pairs and reaches maximum at an altitude of around 10km.

2. Particles emit Cherenkov radiation – around 100 photons per m^2 reaches the ground in a circle of 250m diameter. Flash of Cherenkov light lasts several nanoseconds.

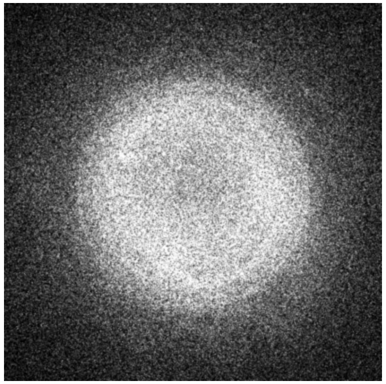

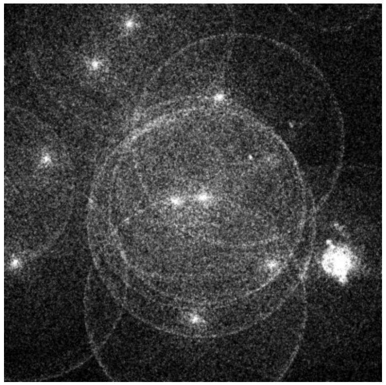

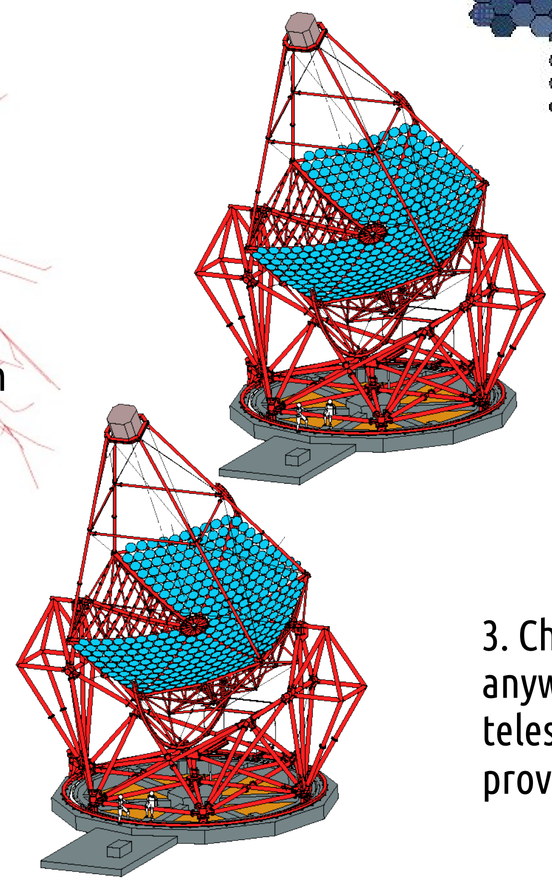

3. Cherenkov photons can be registered anywhere within the cone by an optical telescope (if enough sensitive) – this provides an effective area of **50000 m^2**

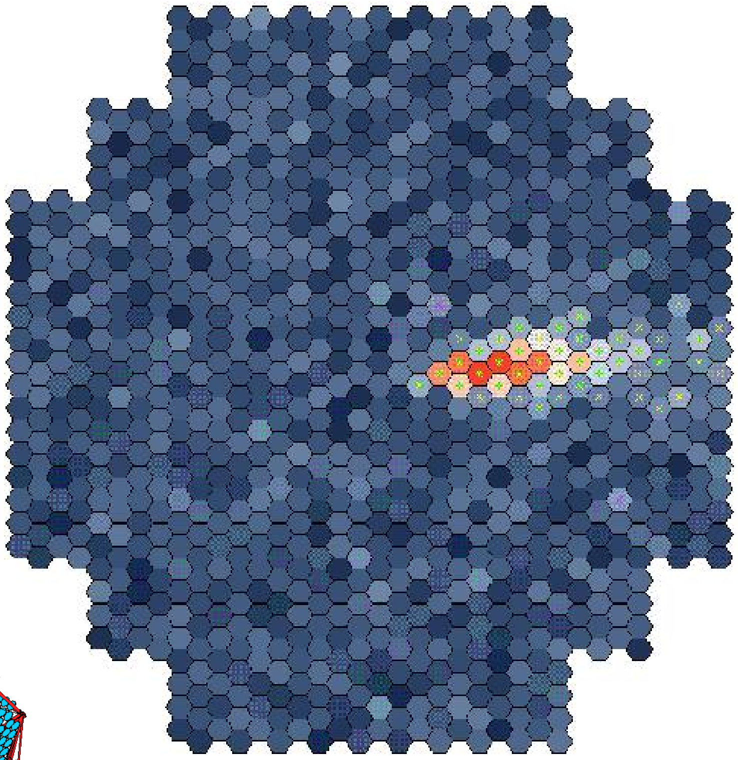

4. Image of the air shower is captured by the camera.

Cherenkov technique - stereoscopy

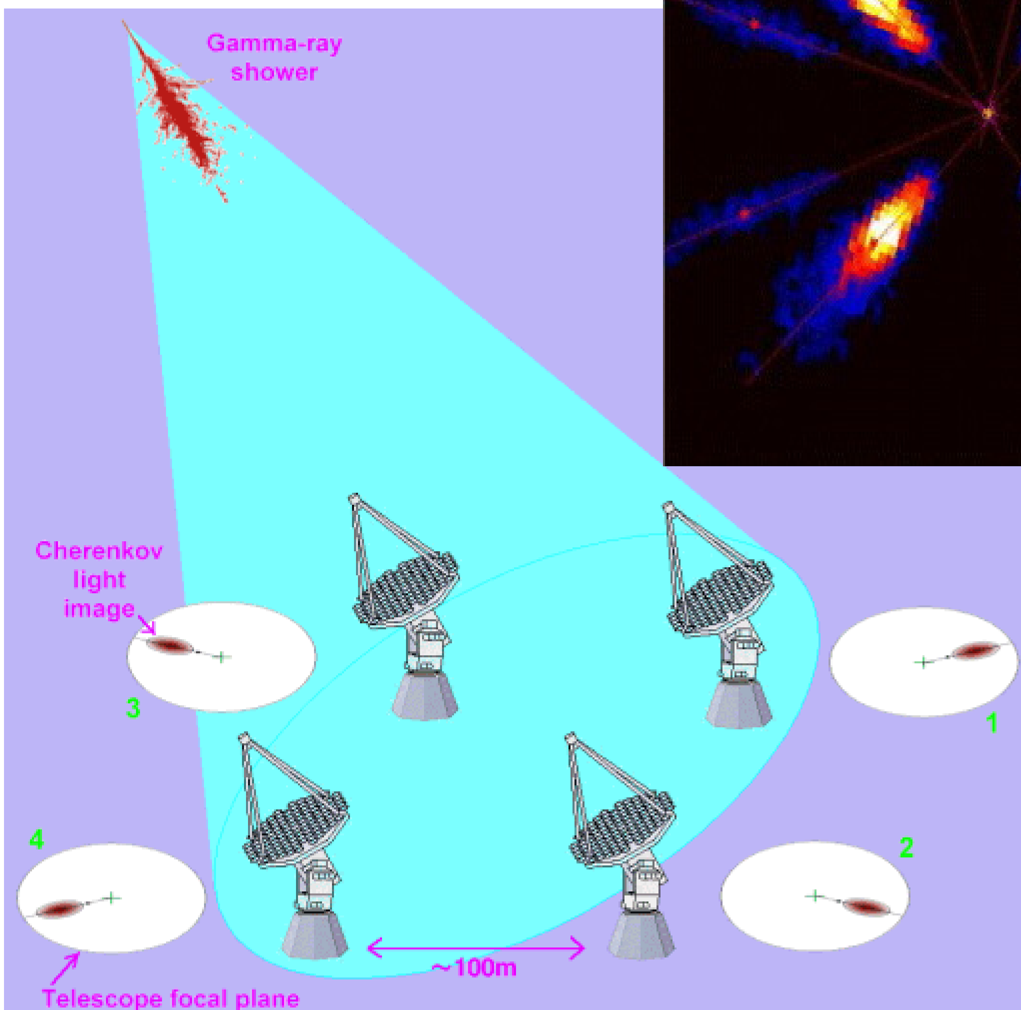

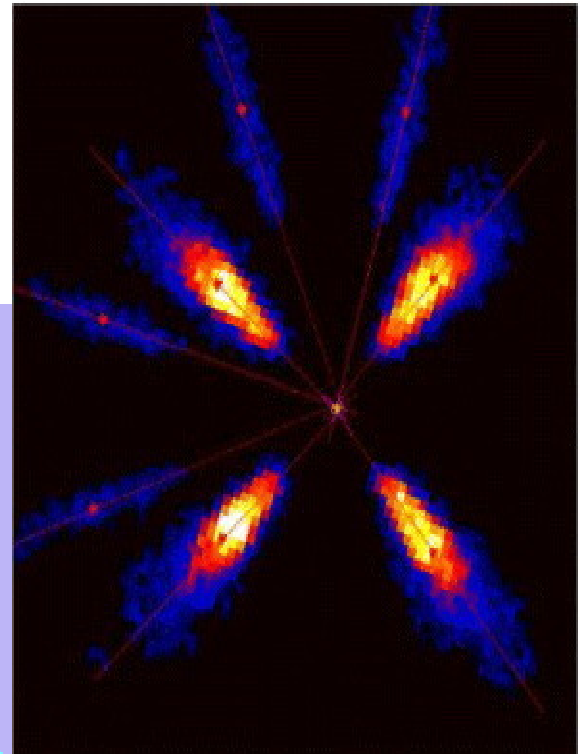

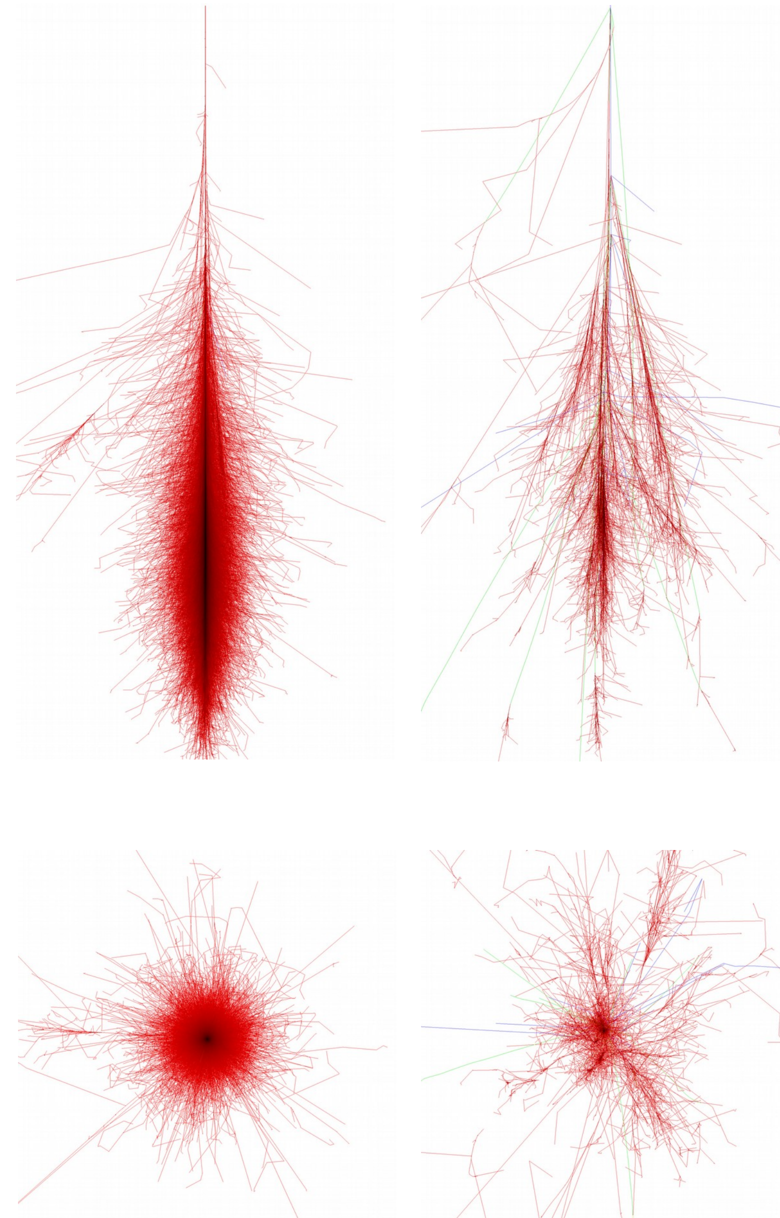

Hardware upgrades

- all CT1-CT4 cameras upgraded to CT1U-CT4U
  - new electronics
  - new light collectors
  - new ventilation system

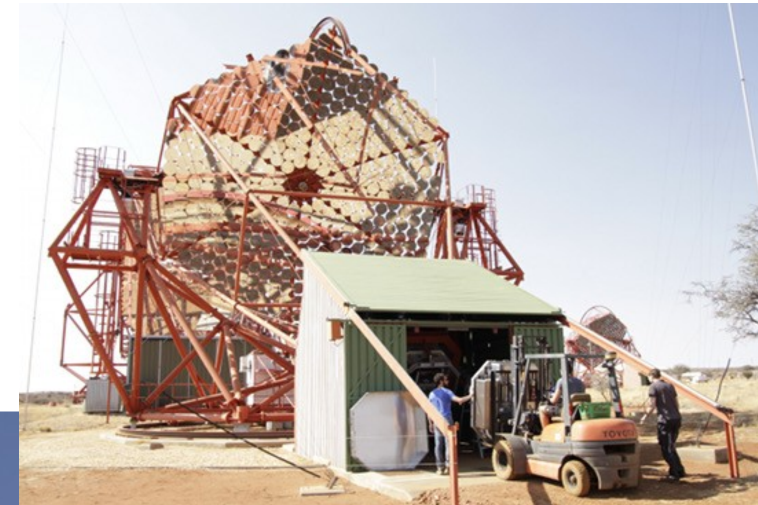

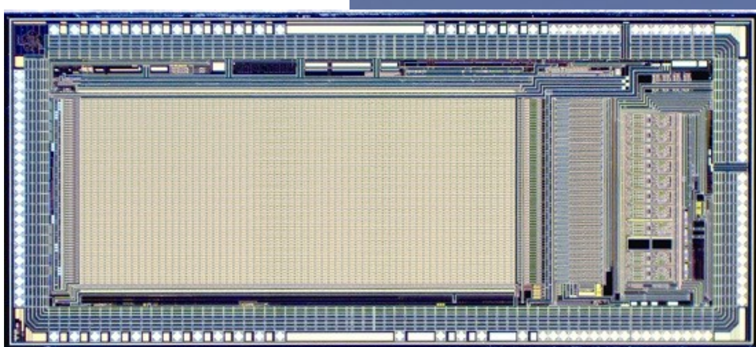

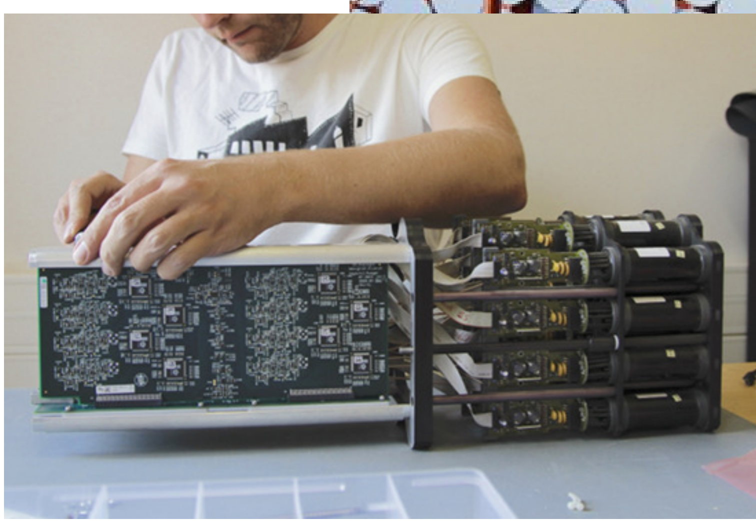

Astroparticle research

Galactic sources:

- supernova remnants (SNRs),
- pulsars and pulsar wind nebulae (PWNs),
- star clusters,
- Galactic centre,
- X-ray binaries (XRBs) and microquasars.

Extragalactic sources:

- active galactic nuclei (AGNs),
- dwarf galaxies (DSs),
- extragalactic background light (EBL),
- gamma-ray bursts (GRBs),
- clusters of galaxies.

Fundamental physics:

- dark matter (DM),
- Lorentz invariance violation (LIV),
- **cosmic-rays (CR)**.

Physical processes:

- particle acceleration to the highest energies,
- particle and radiation propagation in the intergalactic medium,
- structure of the magnetic field at different scales,
- radiation production mechanisms at high energy.

H.E.S.S. - some results

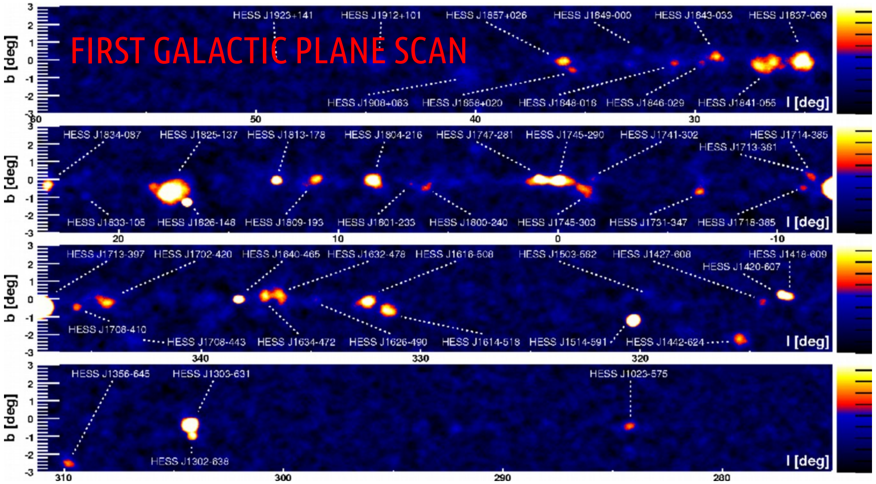

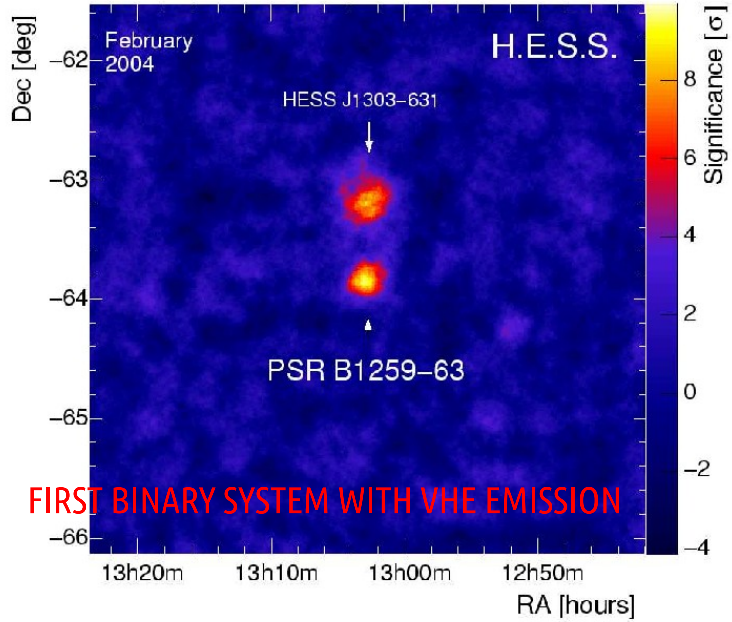

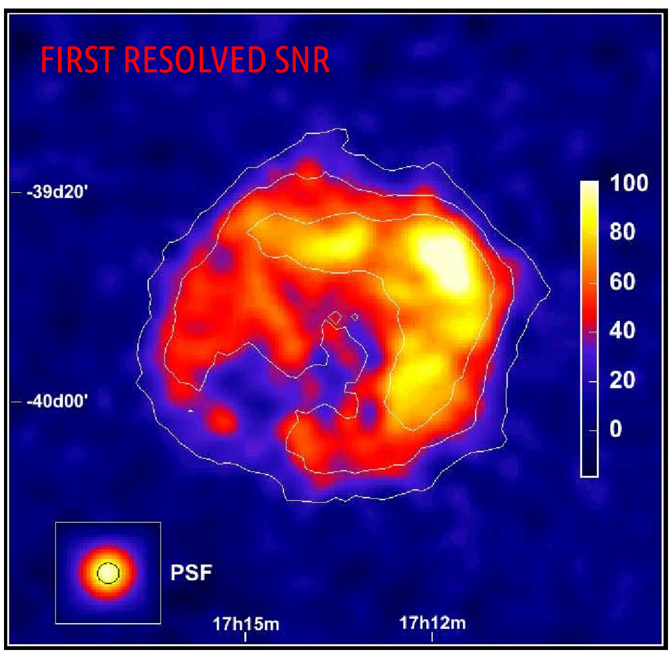

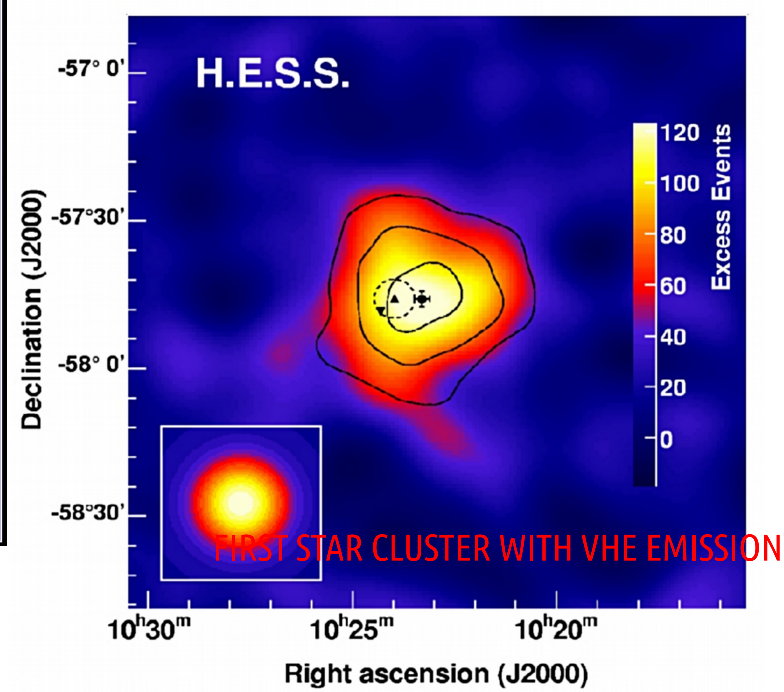

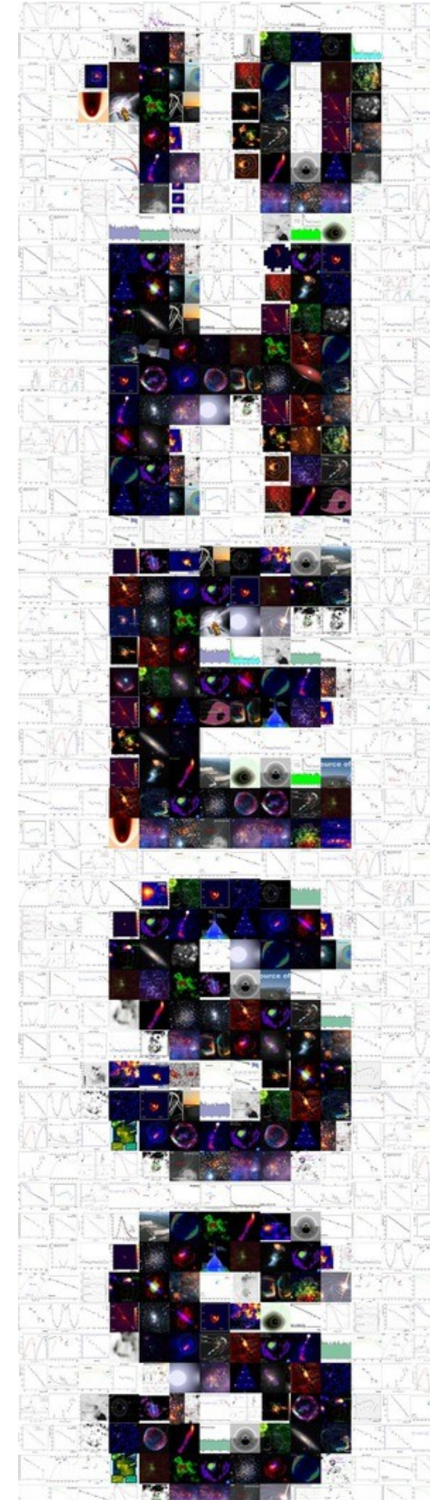

First AGNs detected by H.E.S.S. II (mono)

PG 1553+113

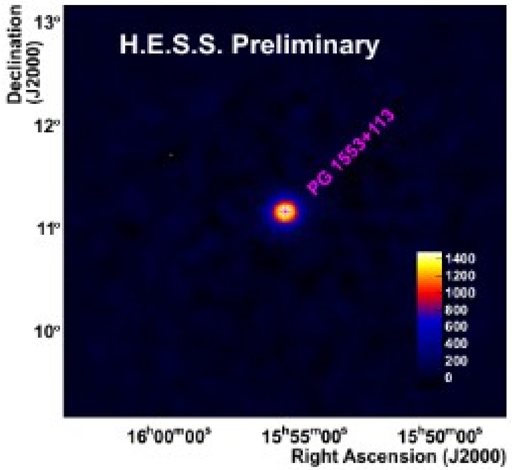

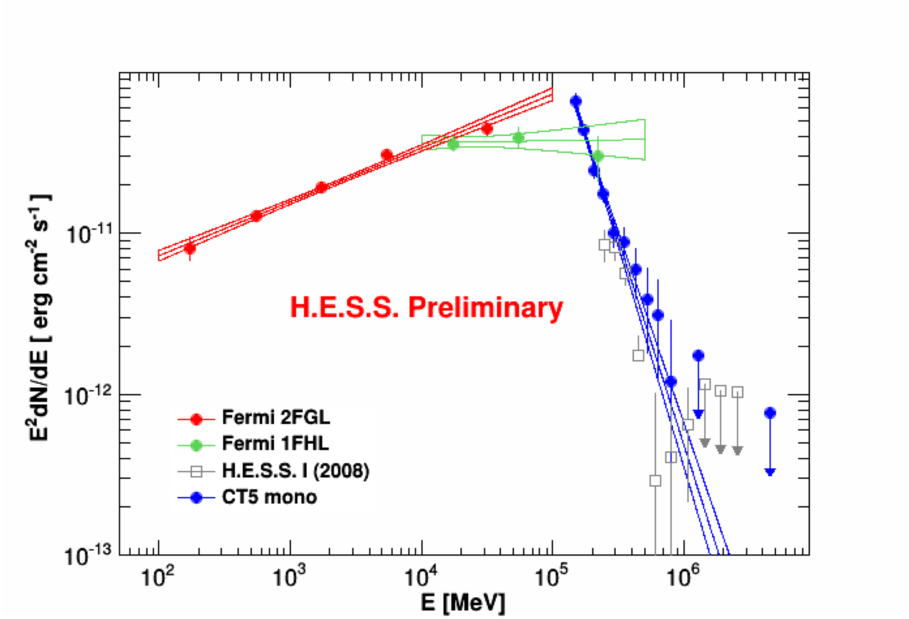

PKS 2155-304

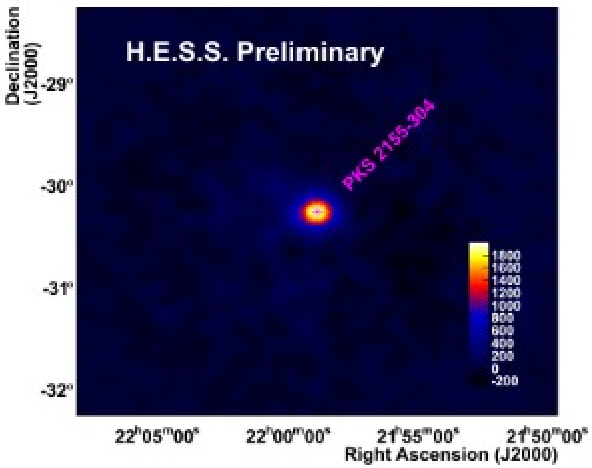

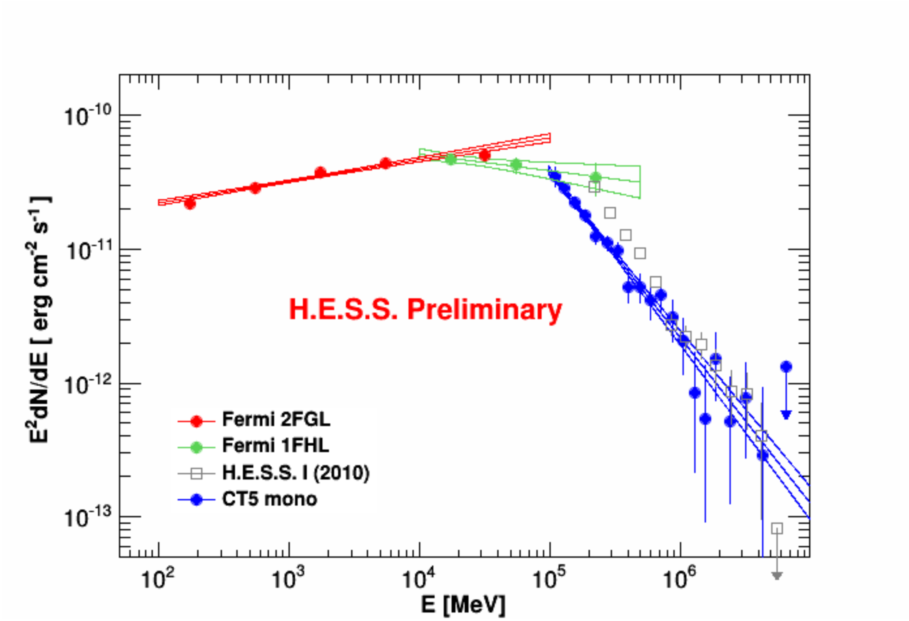

CT5 mono observations

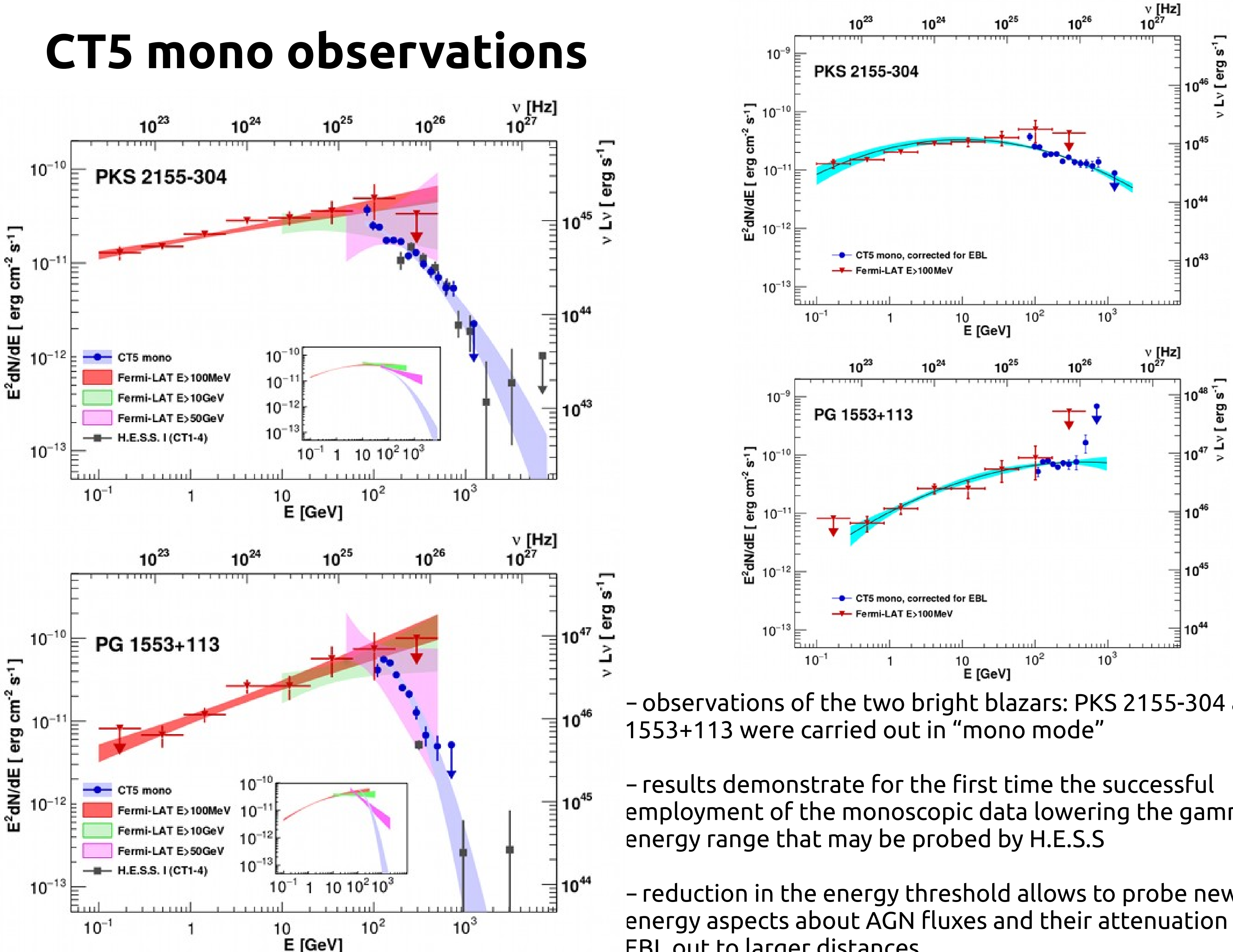

– observations of the two bright blazars: PKS 2155-304 and PG 1553+113 were carried out in "mono mode"

– results demonstrate for the first time the successful employment of the monoscopic data lowering the gamma-ray energy range that may be probed by H.E.S.S

– reduction in the energy threshold allows to probe new low-energy aspects about AGN fluxes and their attenuation on the EBL out to larger distances

CT5 in mono mode - discovery

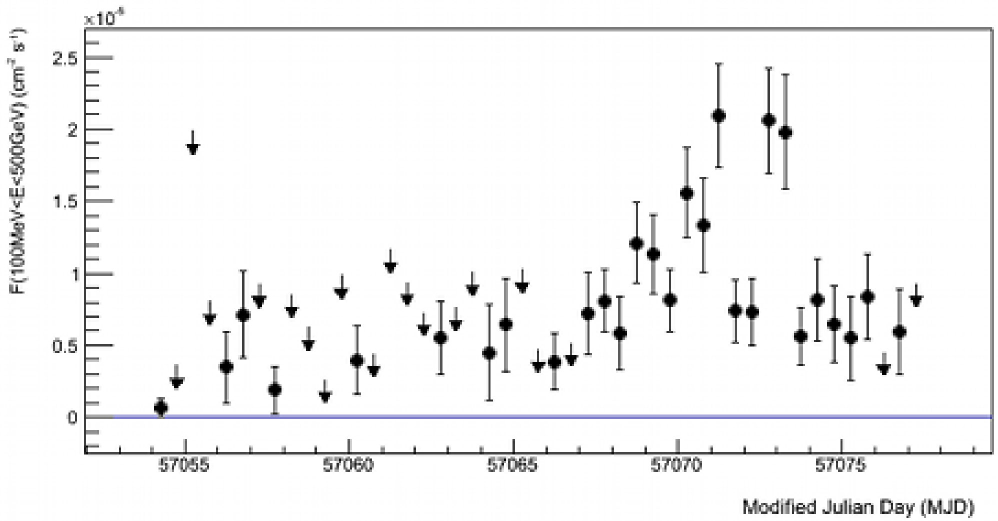

– in February 2015, the FSRQ PKS 0736+017 (z=0.189) underwent a bright flaring episode at high energy (MeV to GeV) gamma rays, as observed with the Fermi LAT,

– the first H.E.S.S. II discovery of a new extragalactic VHE gamma-ray source

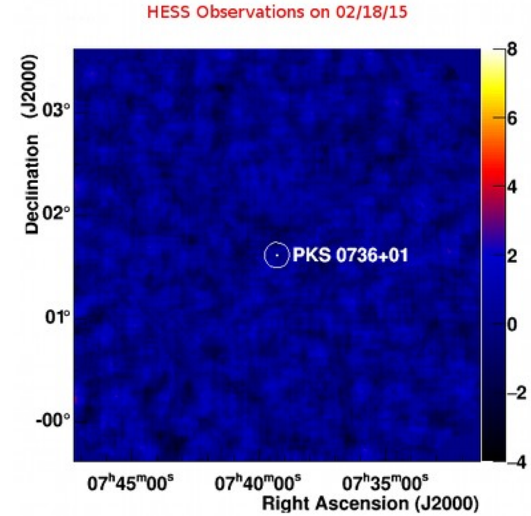

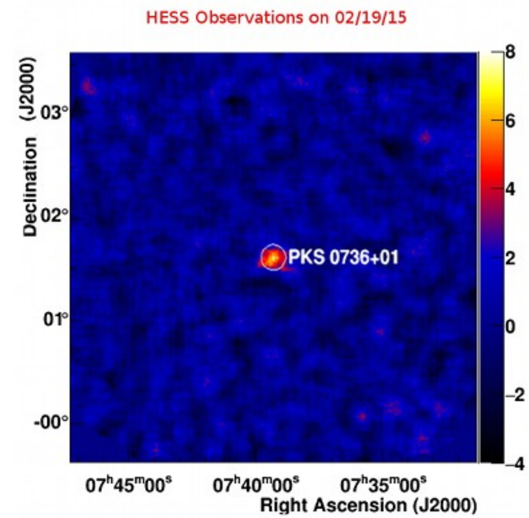

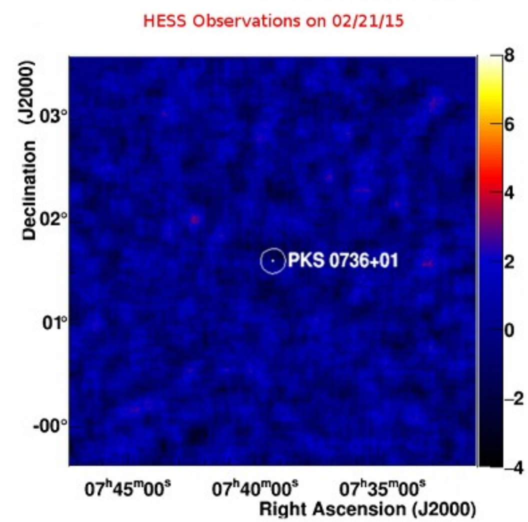

SNR RX J1713.7-3946

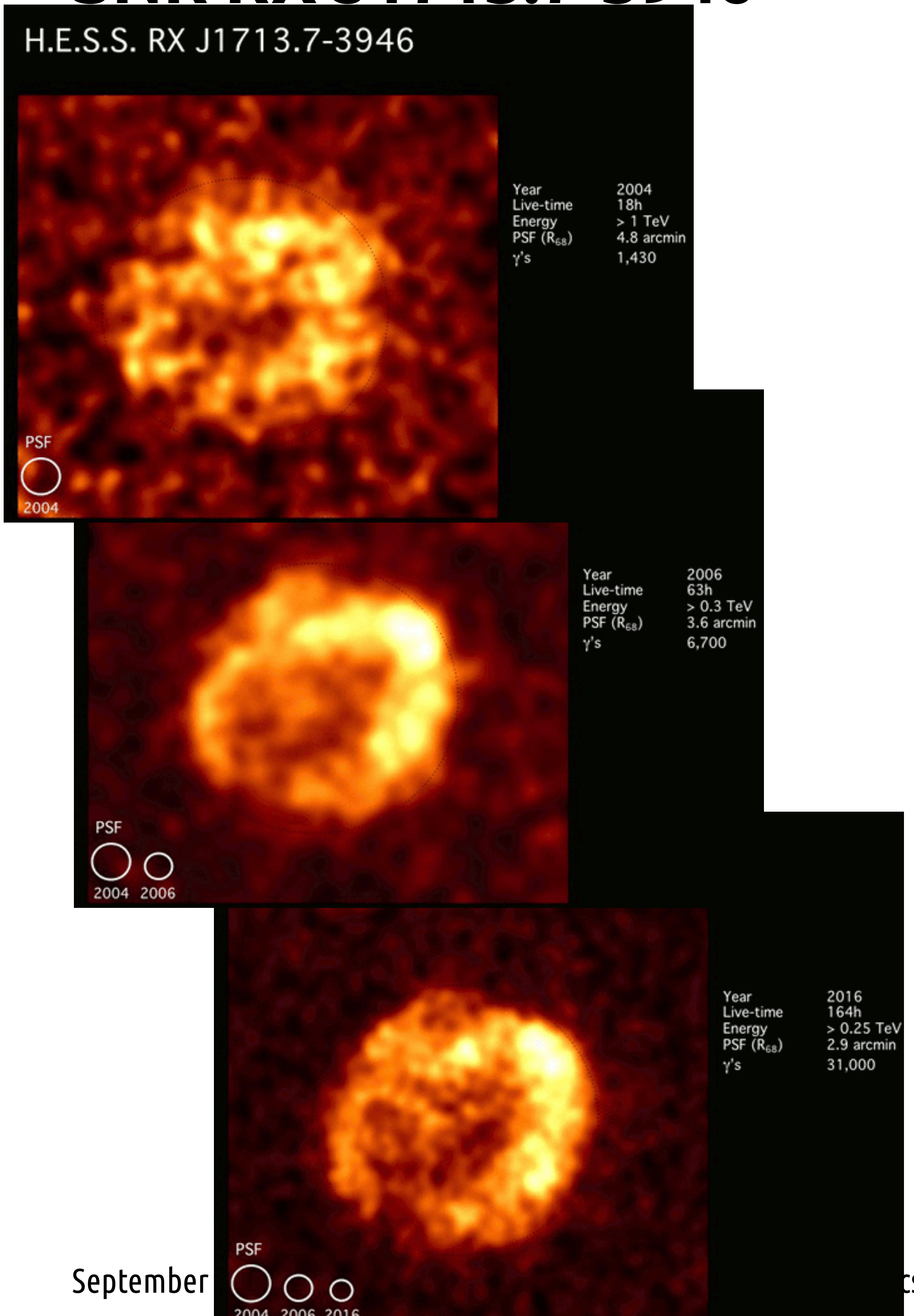

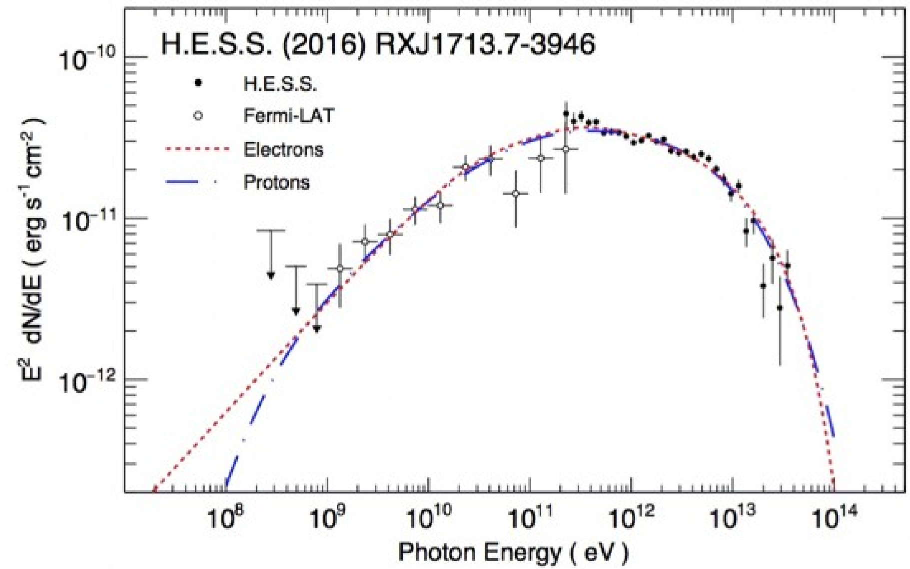

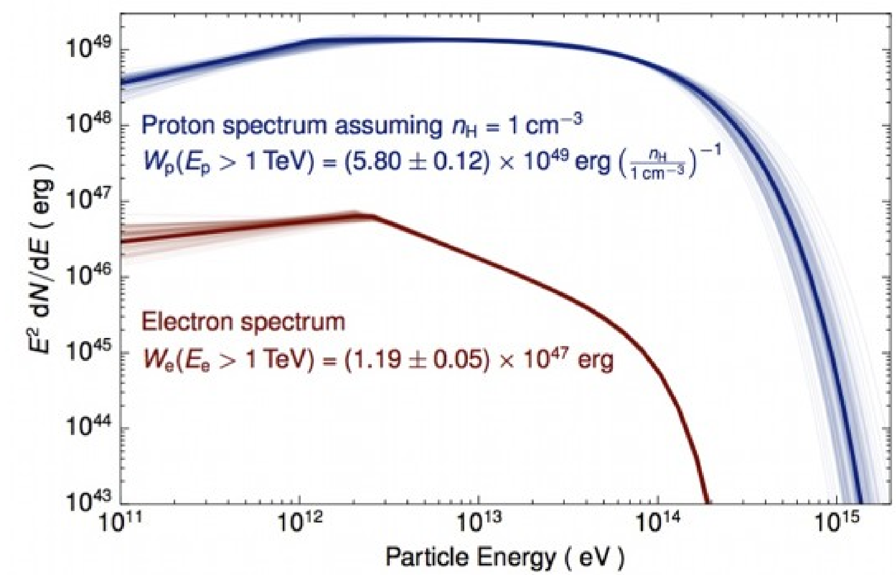

SNR RX J1713.7-3946

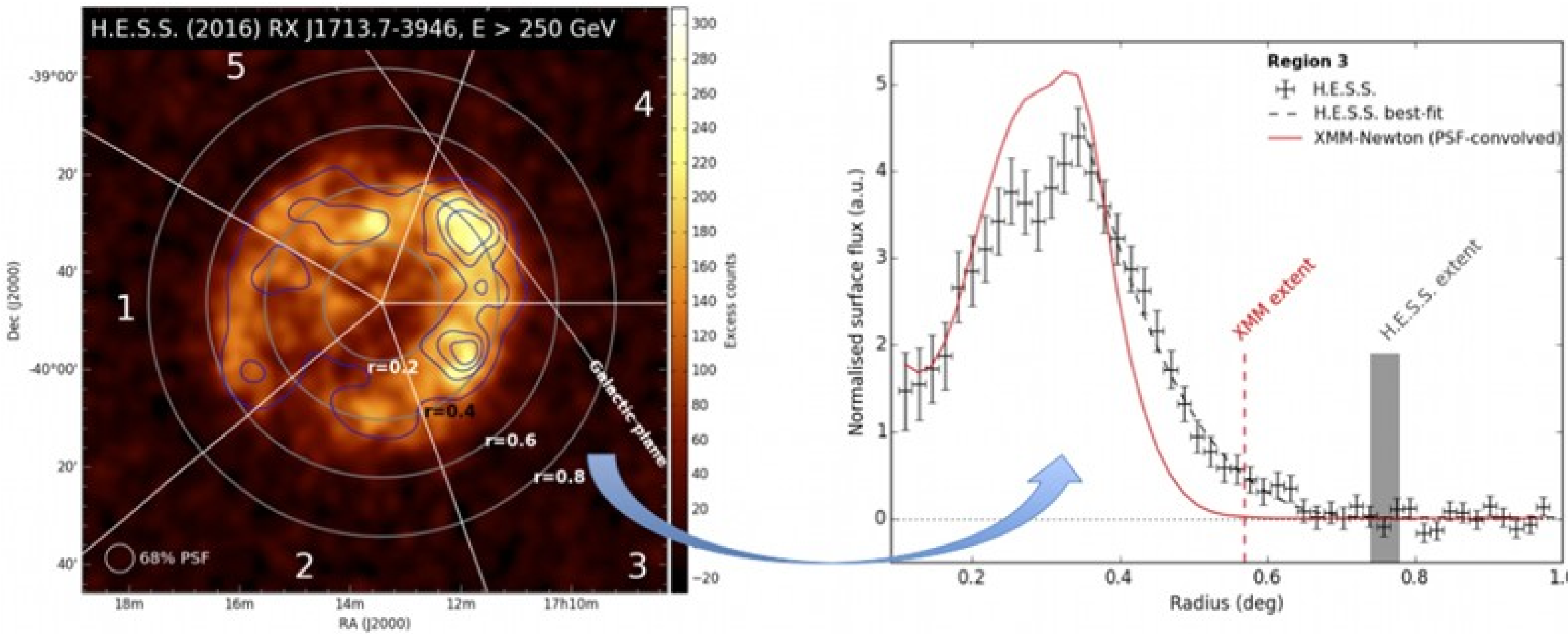

– the radial size of the supernova shell of RX J1713.7-3946 in gamma-rays extends further than in X-rays

– effects from accelerated particles leaving the main shock region have been predicted in diffusive shock acceleration theory: the X-rays mark the end of the shock region, the gamma rays are either from completely detached (escaped) particles or else from particles in the forward shock (shock precursor) region

Vela Junior

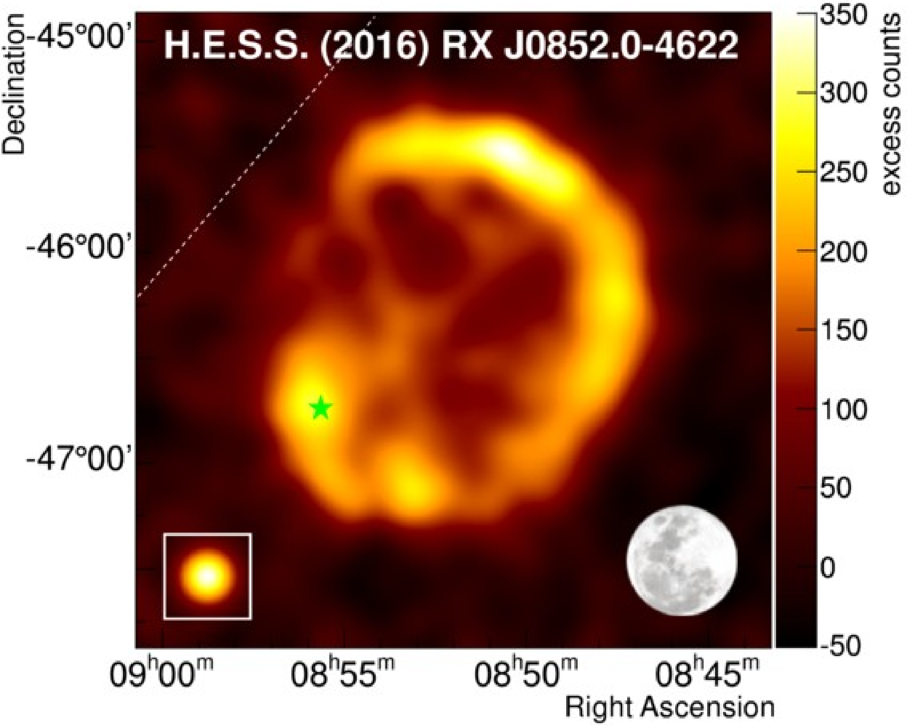

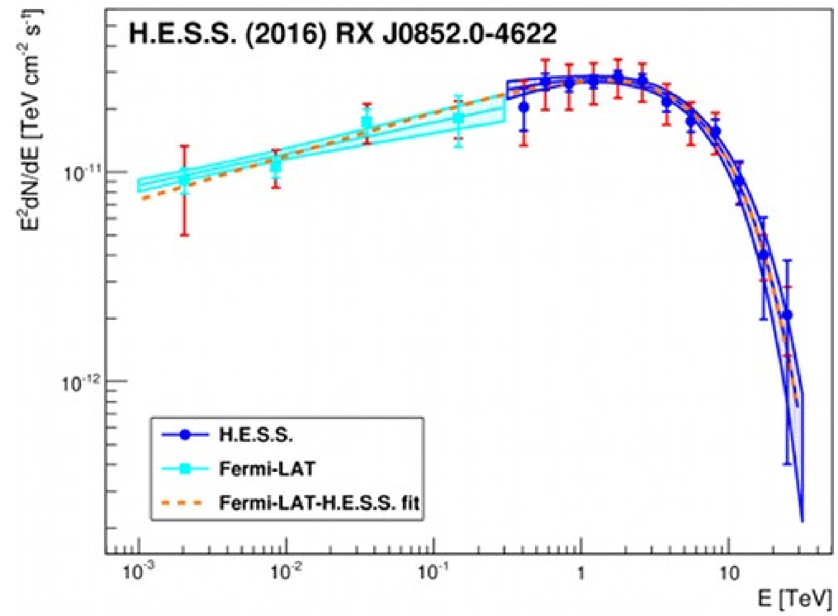

– no clear preference for either leptonic or hadronic scenario

– in the leptonic case, the magnetic field strength within the Vela Junior region is relatively low - 7 μG

– in a hadronic scenario, the total amount of energy in accelerated protons is less than about 10% of the SNR explosion energy; ambient medium density - 1 cm^{-3}

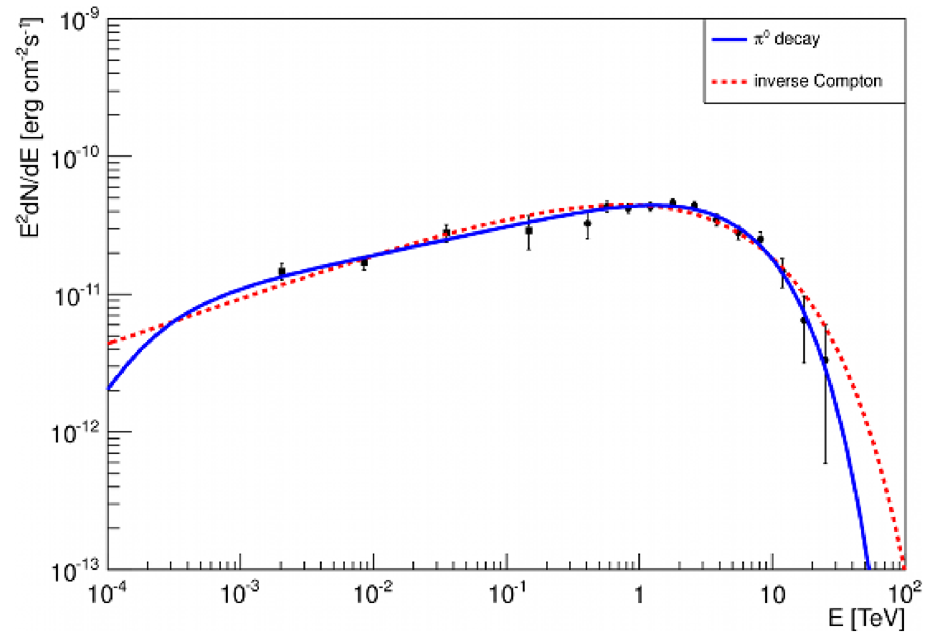

Galactic Plane Scan

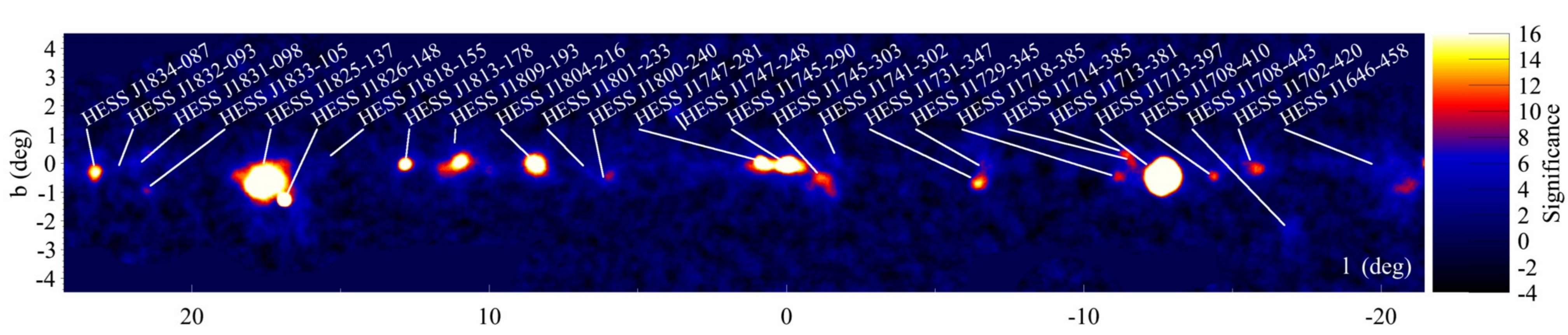

– survey of +/- 3° lat and 250°-70° long
– over 2350h exposure
– over 50 sources (79 in official H.E.S.S. catalog including extragalactic)

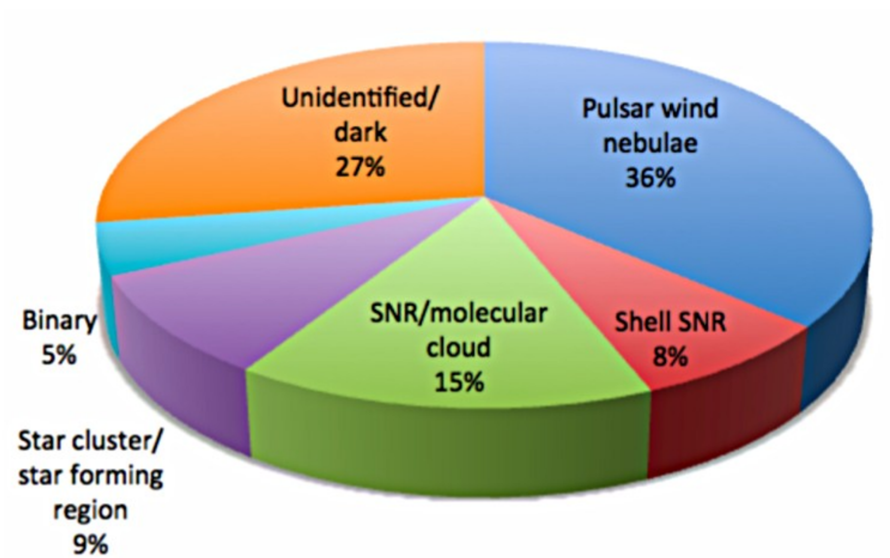

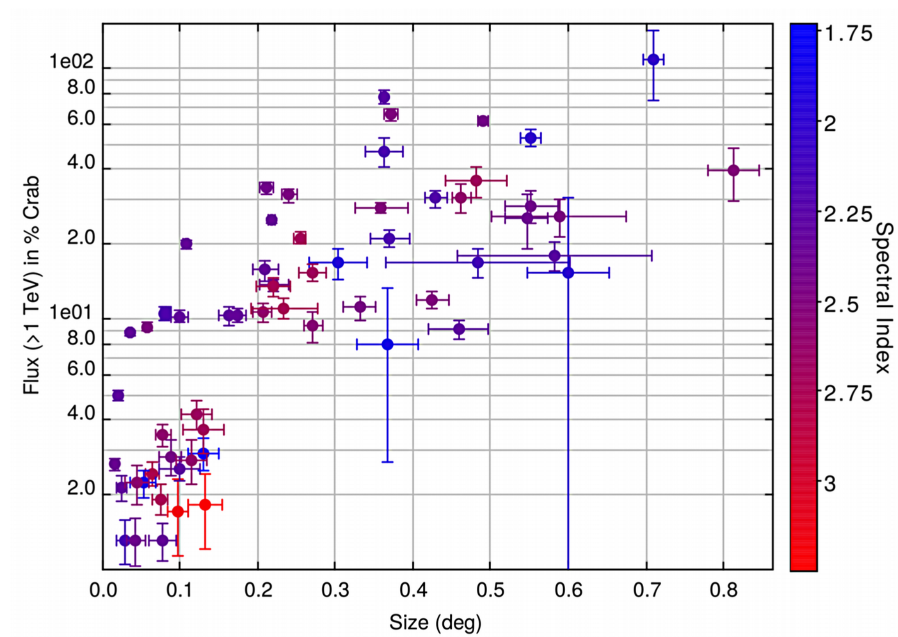

Fig. 17. Size – flux scatter plot for the sources in the HGPS, with spectral index shown in color. The size-dependent sensitivity of the survey is clearly visible; the detection threshold is higher at higher flux for larger sources. The fact that there are no sources in the upper left corner is not a selection effect, a source located there would have been detected.

Galactic Plane Scan

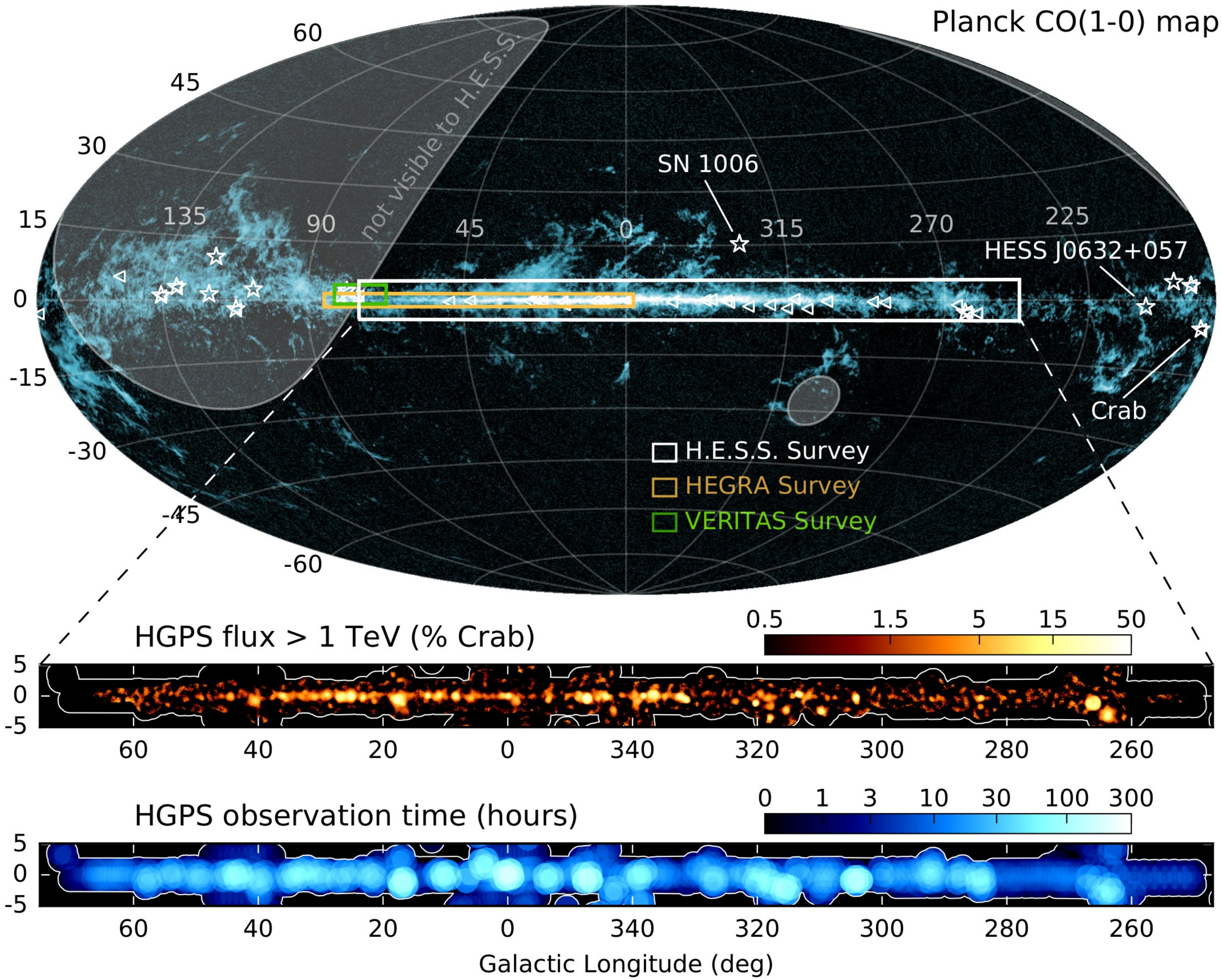

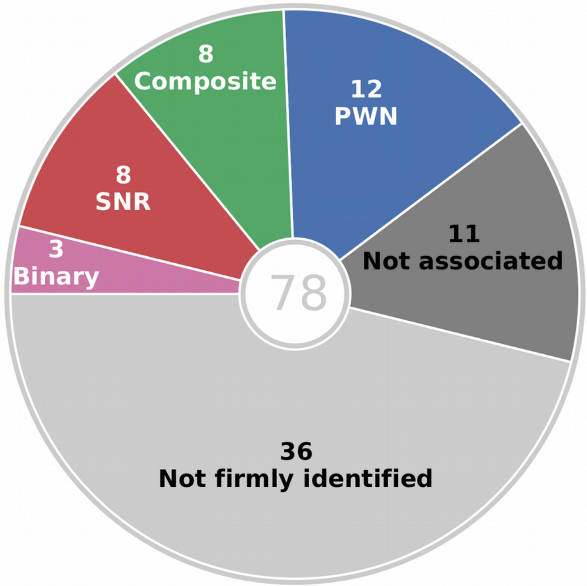

– survey of +/- 3° lat and 250°-70° long
– over 2700 h exposure
– 78 sources

HGPS

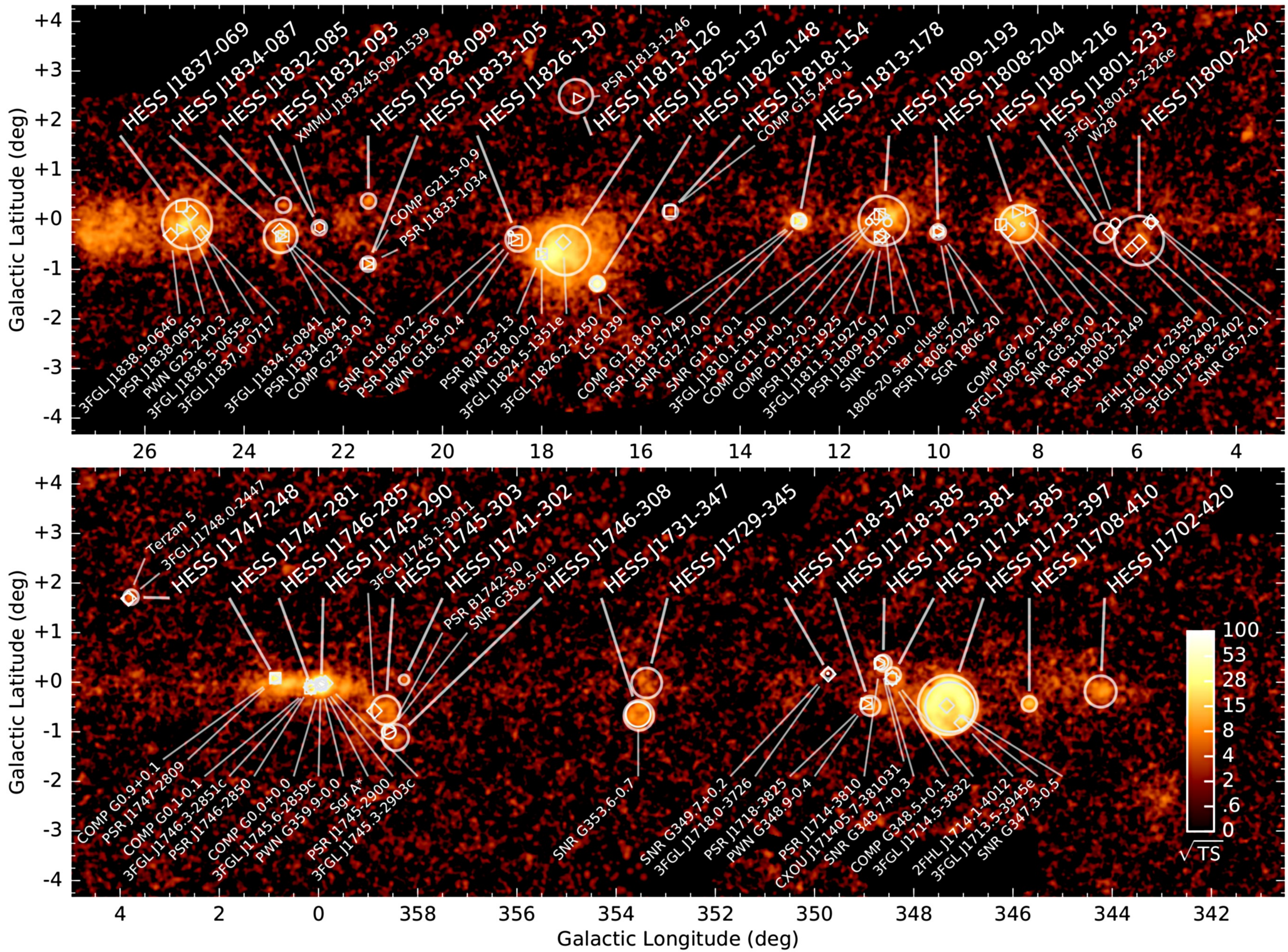

Galactic Latitude (deg)
Galactic Longitude (deg)
HESS J1837-069
HESS J1834-087
HESS J1832-085
HESS J1832-093
XMMU J183245-0921539
HESS J1828-099
HESS J1833-105
HESS J1826-130
PSR J1813-1246
HESS J1813-126
HESS J1825-137
HESS J1826-148
HESS J1818-154
COMP G15.4+0.1
HESS J1813-178
HESS J1809-193
HESS J1808-204
HESS J1804-216
HESS J1801-233
3FGL J1801.3-2326e
W28
HESS J1800-240
COMP G21.5-0.9
PSR J1833-1034
3FGL J1838.9-0646
PSR J1838-0655
PWN G25.2+0.3
3FGL J1836.5-0655e
3FGL J1837.6-0717
3FGL J1834.5-0841
PSR J1834-0845
COMP G23.3-0.3
SNR G18.6-0.2
PSR J1826-1256
PWN G18.5-0.4
PSR B1823-13
PWN G18.0-0.7
3FGL J1824.5-1351e
3FGL J1826.2-1450
LS 5039
COMP G12.8-0.0
PSR J1813-1749
SNR G12.7-0.0
SNR G11.4-0.1
3FGL J1810.1-1910
COMP G11.1+0.1
COMP G11.2-0.3
PSR J1811-1925
3FGL J1811.3-1927c
PSR J1809-1917
SNR G11.0-0.0
1806-20 star cluster
PSR J1808-2024
SGR 1806-20
COMP G8.7-0.1
3FGL J1805.6-2136e
SNR G8.3-0.0
PSR B1800-21
PSR J1803-2149
2FHL J1801.7-2358
3FGL J1800.8-2402
3FGL J1758.8-2402
SNR G5.7-0.1
Terzan 5
3FGL J1748.0-2447
HESS J1747-248
HESS J1747-281
HESS J1746-285
HESS J1745-290
3FGL J1745.1-3011
HESS J1745-303
HESS J1741-302
PSR B1742-30
SNR G358.5-0.9
HESS J1746-308
HESS J1731-347
HESS J1729-345
HESS J1718-374
HESS J1718-385
HESS J1713-381
HESS J1714-385
HESS J1713-397
HESS J1708-410
HESS J1702-420
COMP G0.9+0.1
PSR J1747-2809
COMP G0.1-0.1
3FGL J1746.3-2851c
PSR J1746-2850
COMP G0.0+0.0
3FGL J1745.6-2859c
PWN G359.9-0.0
Sgr A*
PSR J1745-2900
3FGL J1745.3-2903c
SNR G353.6-0.7
SNR G349.7+0.2
3FGL J1718.0-3726
PSR J1718-3825
PWN G348.9-0.4
PSR J1714-3810
CXOU J171405.7-381031
SNR G348.7+0.3
COMP G348.5+0.1
3FGL J1714.5-3832
2FHL J1714.1-4012
3FGL J1713.5-3945e
SNR G347.3-0.5
√TS

Galactic Centre

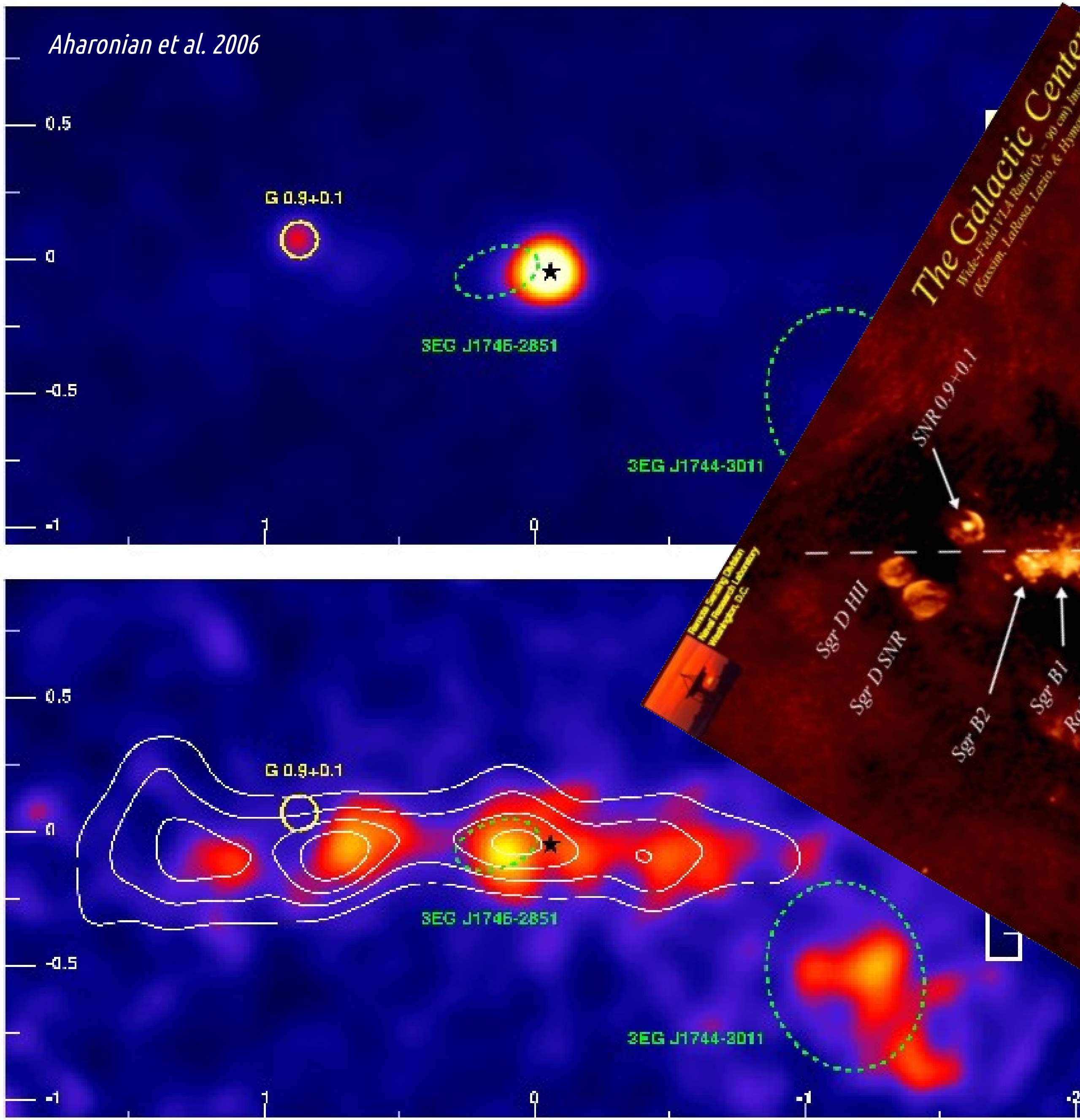

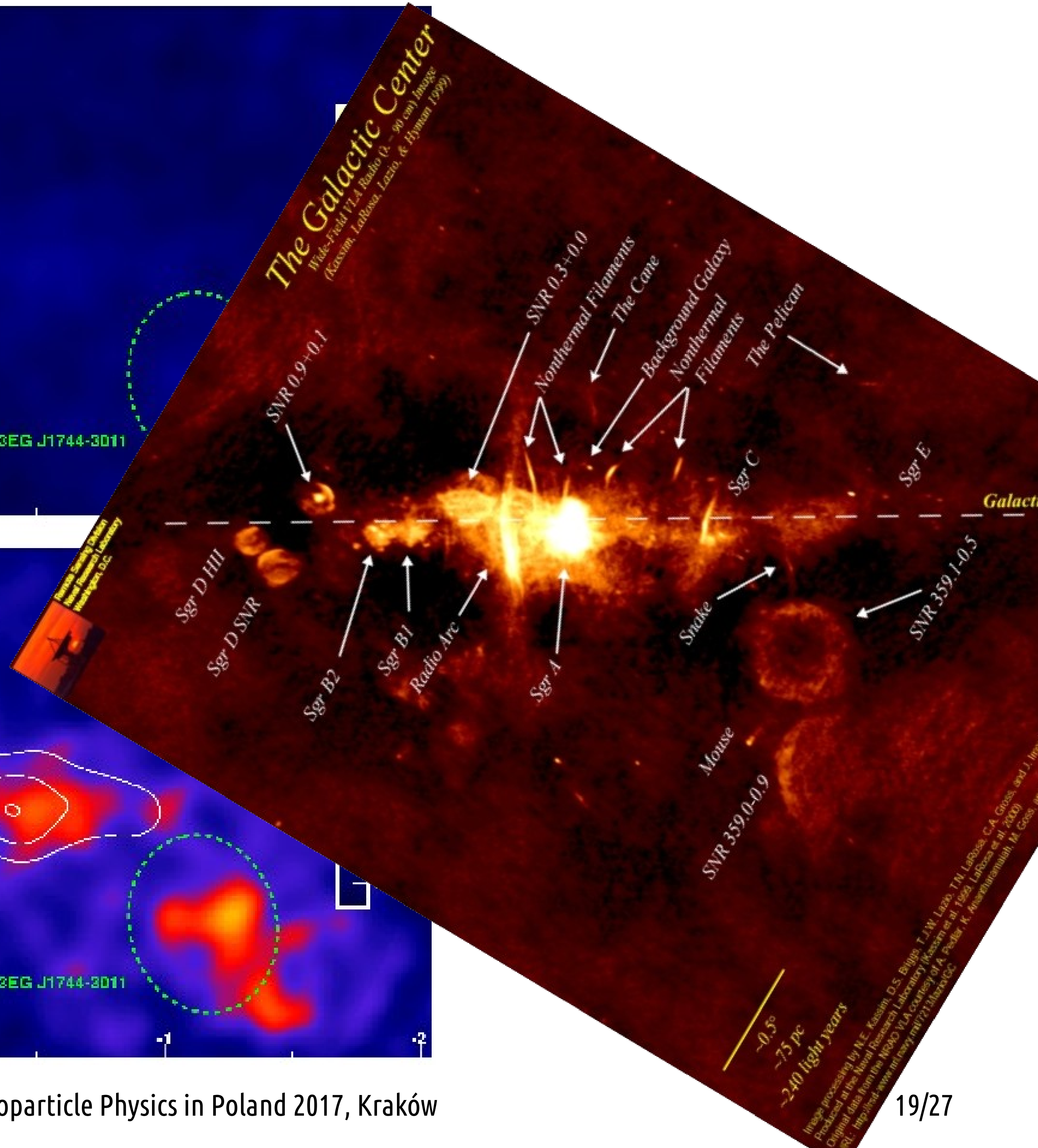

Galactic Centre with H.E.S.S.

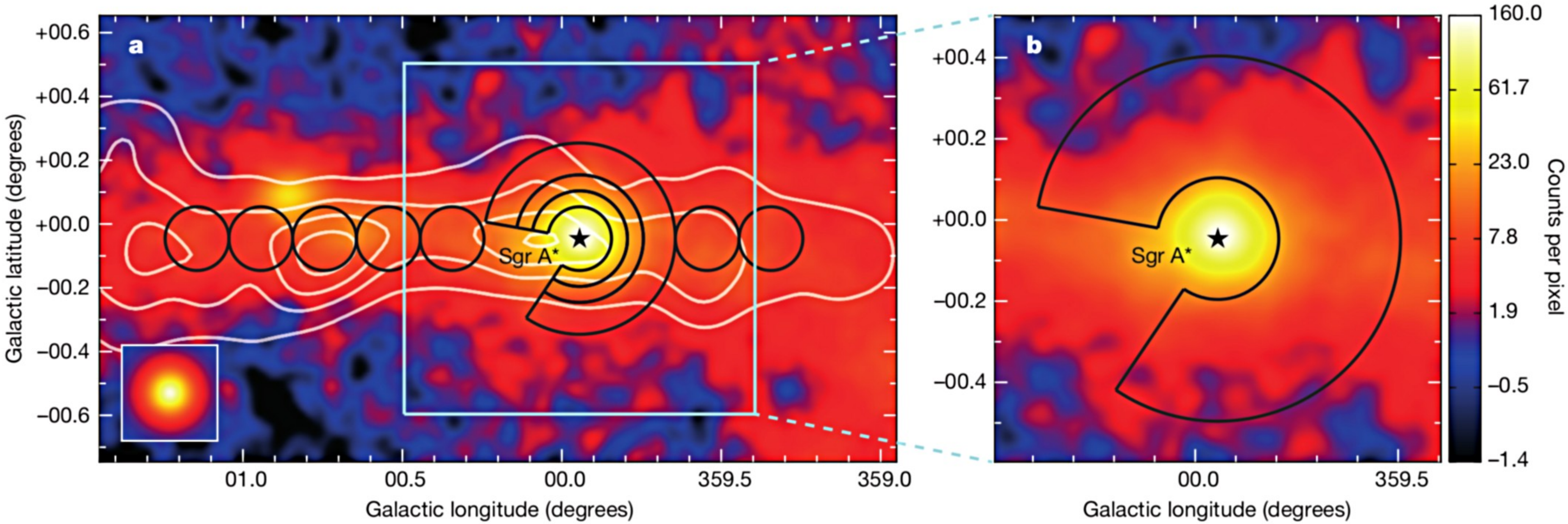

Figure 1 | VHE γ-ray image of the Galactic Centre region. The colour scale indicates counts per $0.02° \times 0.02°$ pixel. **a**, The black lines outline the regions used to calculate the cosmic-ray energy density throughout the central molecular zone. A section of 66° is excluded from the annuli (see Methods). White contour lines indicate the density distribution of molecular gas, as traced by its CS line emission[30]. Black star, location of Sgr A*. Inset (bottom left), simulation of a point-like source. The part of the image shown boxed is magnified in **b**. **b**, Zoomed view of the inner ∼70 pc and the contour of the region used to extract the spectrum of the diffuse emission.

- molecular clouds (+250pc,-150pc)
- gamma-ray emission correlated with clouds density

Galactic Centre with H.E.S.S.

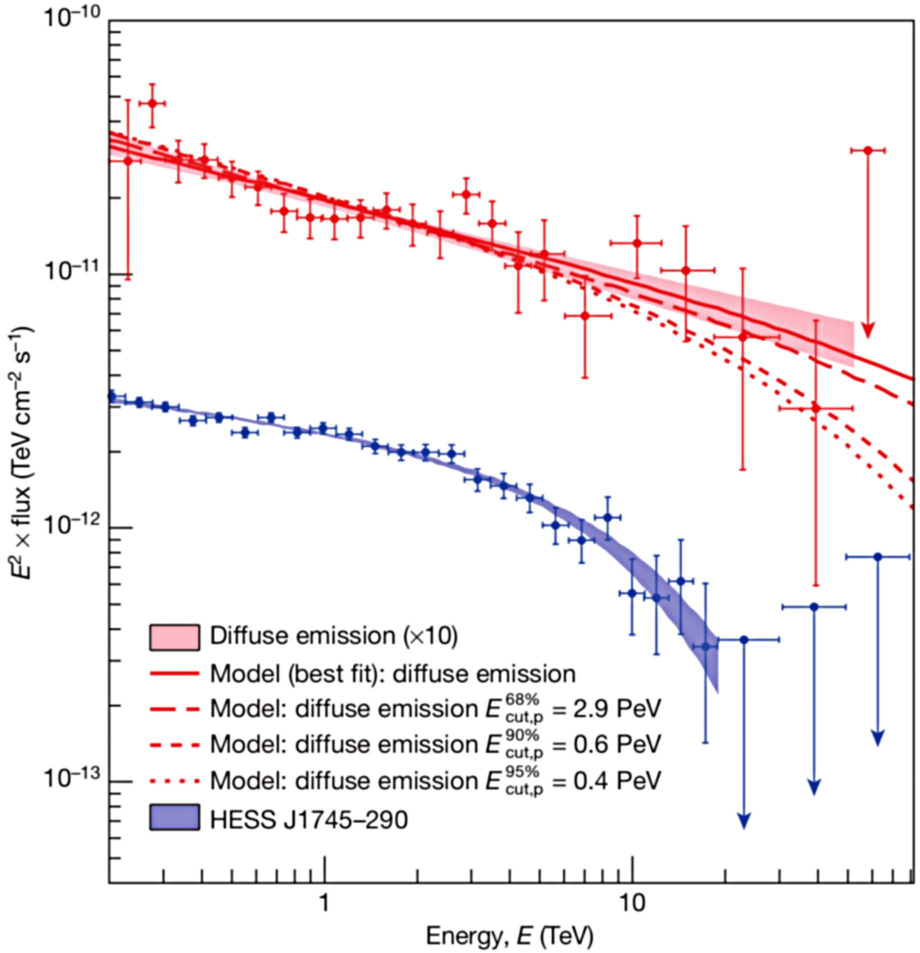

Figure 3 | VHE γ-ray spectra of the diffuse emission and HESS J1745−290. The y axis shows fluxes multiplied by a factor E^2, where E is the energy on the x axis, in units of TeV cm^{-2} s^{-1}. The vertical and horizontal error bars show the 1σ statistical error and the bin size, respectively. Arrows represent 2σ flux upper limits. The 1σ confidence bands of the best-fit spectra of the diffuse and HESS J1745−290 are shown in red and blue shaded areas, respectively. Spectral parameters are given in Methods. The red lines show the numerical computations assuming that γ-rays result from the decay of neutral pions produced by proton–proton interactions. The fluxes of the diffuse emission spectrum and models are multiplied by 10.

$dN/dE=\Phi_0 E^{-\Gamma}$; Φ_0 = 2 x 10^{-12} TeV^{-1} cm^{-2} s^{-1}; **Γ=2.3**;
L_γ(>1TeV)=5.7 x 10^{37} erg s^{-1}

leptonic model – inverse Compton emission from relativistic electrons

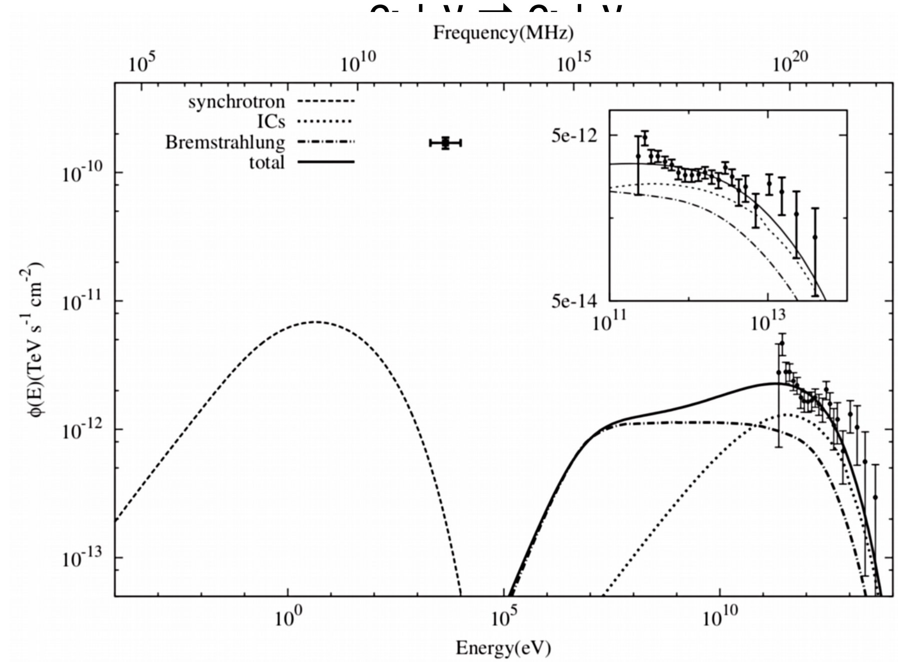

t_{diff}=2x10^3 (R/200pc)^2 (D/10^{30}cm^2 s^{-1}) lat

t_{synch}=10 (B/100μG)$^{-2}$ (E/100TeV)$^{-1}$ lat

Galactic Centre with H.E.S.S.

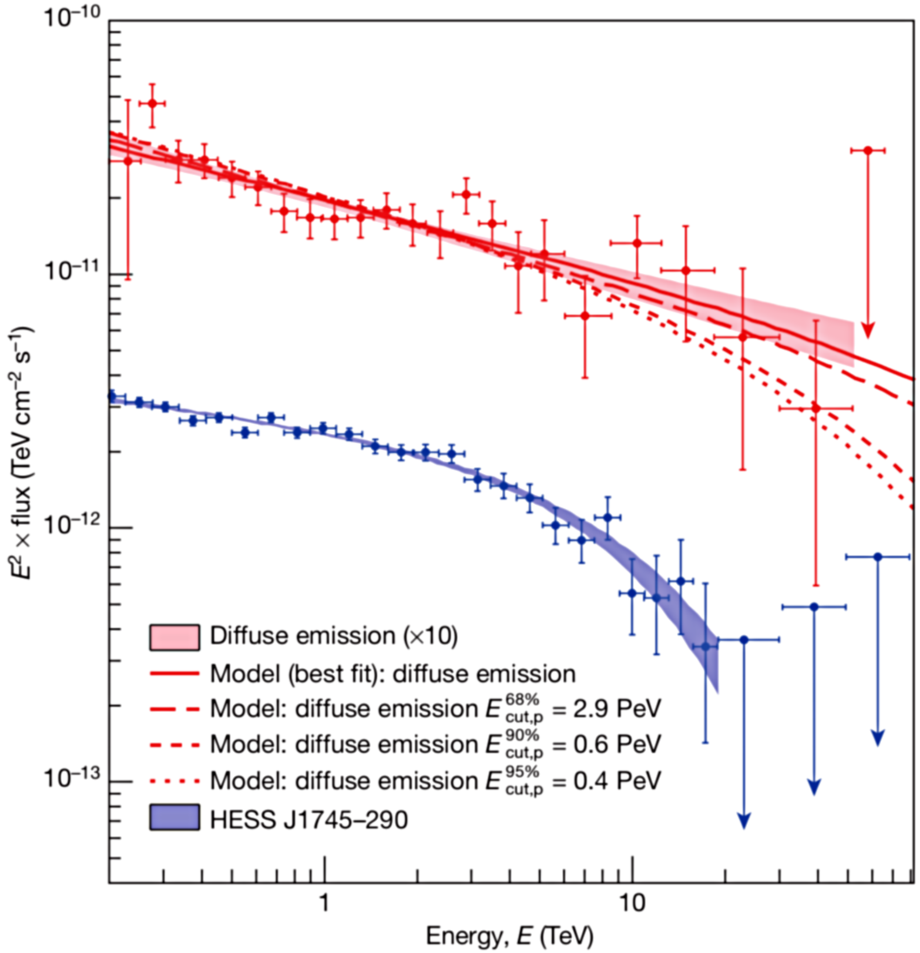

Figure 3 | VHE γ-ray spectra of the diffuse emission and HESS J1745−290. The y axis shows fluxes multiplied by a factor E^2, where E is the energy on the x axis, in units of TeV cm^{-2} s^{-1}. The vertical and horizontal error bars show the 1σ statistical error and the bin size, respectively. Arrows represent 2σ flux upper limits. The 1σ confidence bands of the best-fit spectra of the diffuse and HESS J1745−290 are shown in red and blue shaded areas, respectively. Spectral parameters are given in Methods. The red lines show the numerical computations assuming that γ-rays result from the decay of neutral pions produced by proton–proton interactions. The fluxes of the diffuse emission spectrum and models are multiplied by 10.

hadronic model – proton-proton interactions

$p + p \rightarrow \Pi^0 + \ldots \qquad \Pi^0 \rightarrow \gamma\gamma$

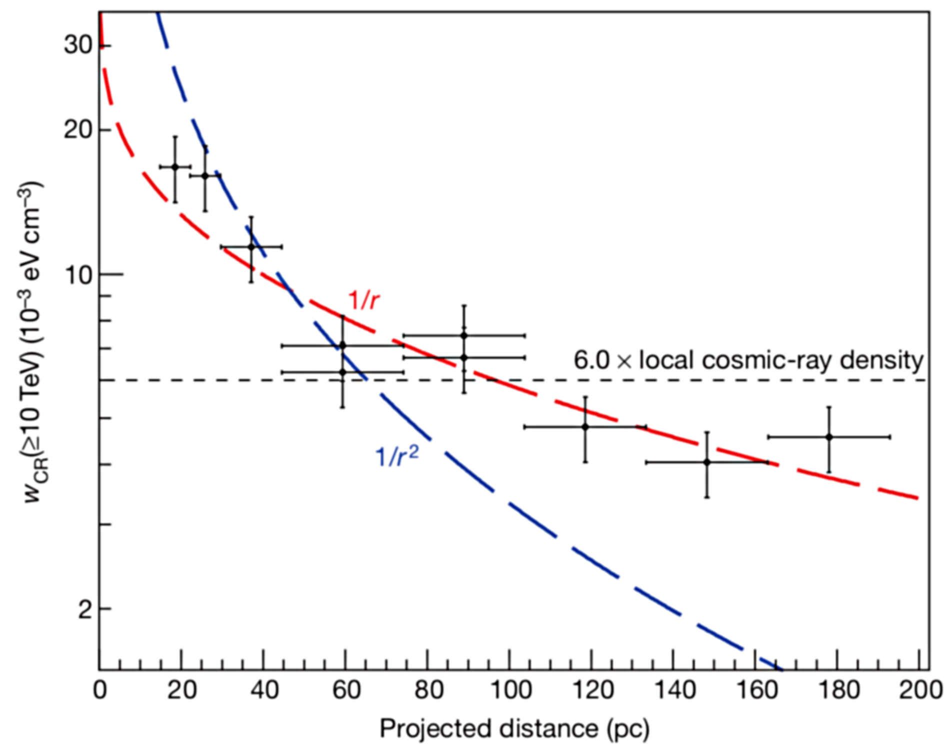

Figure 2 | Spatial distribution of the cosmic-ray density versus projected distance from Sgr A*. The vertical and horizontal error bars show the 1σ statistical plus systematic errors and the bin size, respectively. Fits to the data of a $1/r$ (red line, χ^2/d.o.f. = 11.8/9), a $1/r^2$ (blue line, χ^2/d.o.f. = 73.2/9) and a homogeneous (black line, χ^2/d.o.f. = 61.2/9) cosmic-ray density radial profile integrated along the line of sight are shown. The best fit of a $1/r^\alpha$ profile to the data is found for $\alpha = 1.10 \pm 0.12$ (1σ). The $1/r$ radial profile is clearly preferred for the HESS data.

Dark matter in the Galactic halo

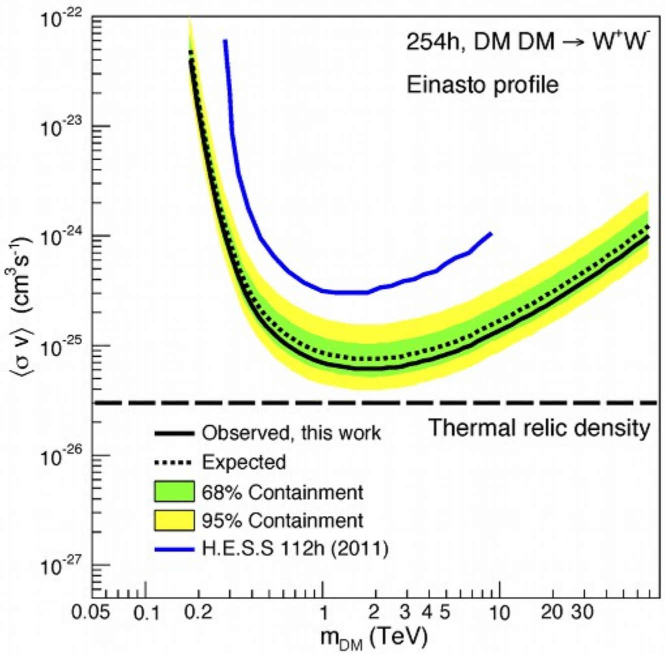

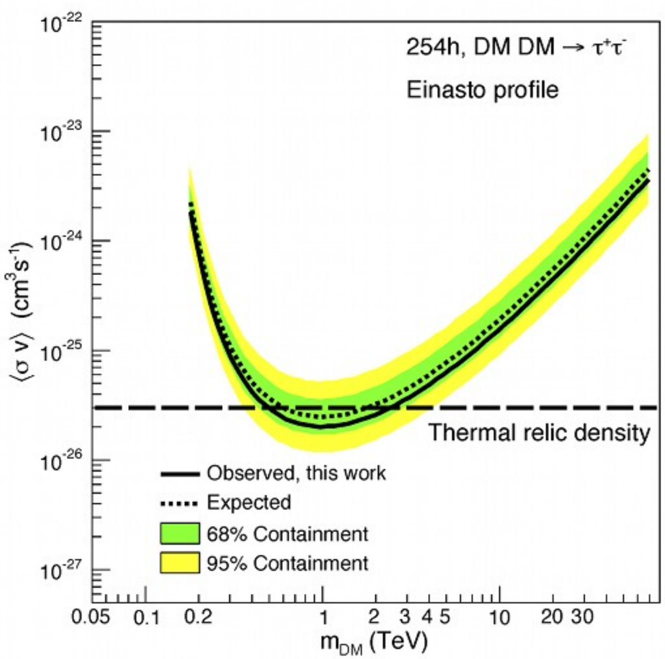

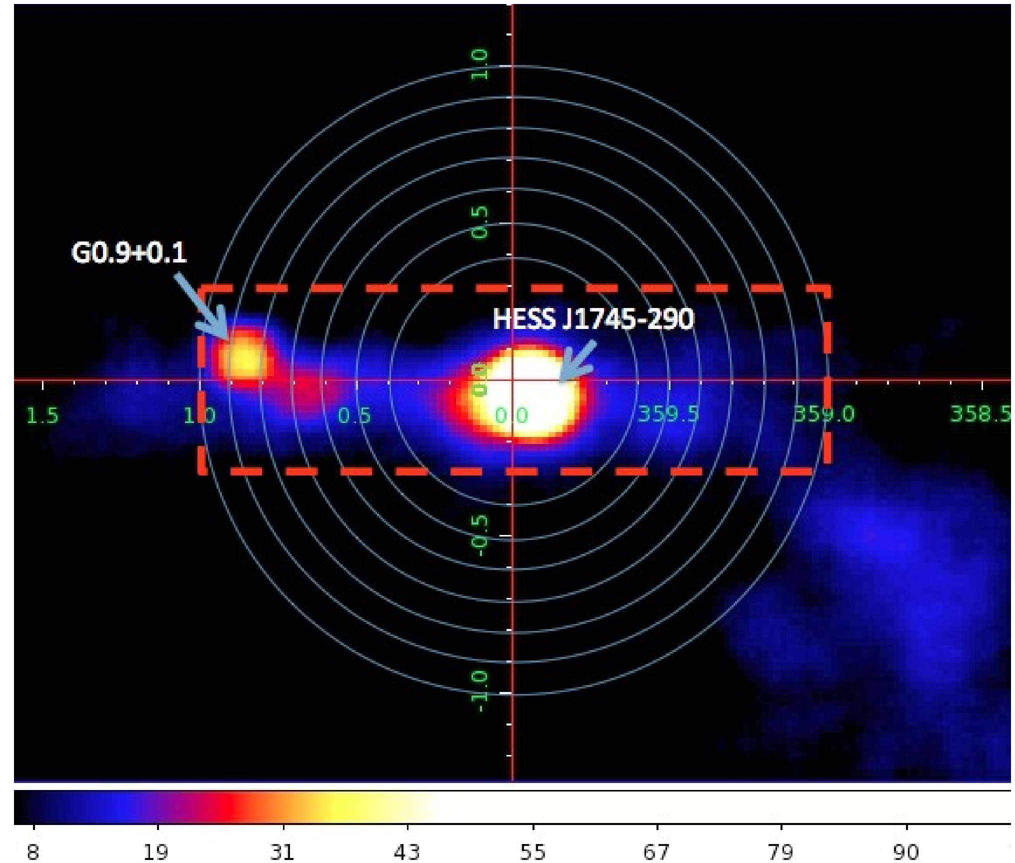

– the inner 300 parsecs region of the Milky Way has been observed by the H.E.S.S. telescopes since 2004

– data analysis does not show any significant gamma-ray excess above the expected background in any of the annuli

– constraints on the DM velocity weighted annihilation cross section can be derived

$$\langle \sigma v \rangle = 6 \times 10^{-26}\ cm^2 s^{-1}$$

at a dark matter mass of 1 TeV for DM DM → W^+W^- channel

130 GeV line

C. Weniger, J. Cosmol. Astropart. Phys. 08 (2012) 007.

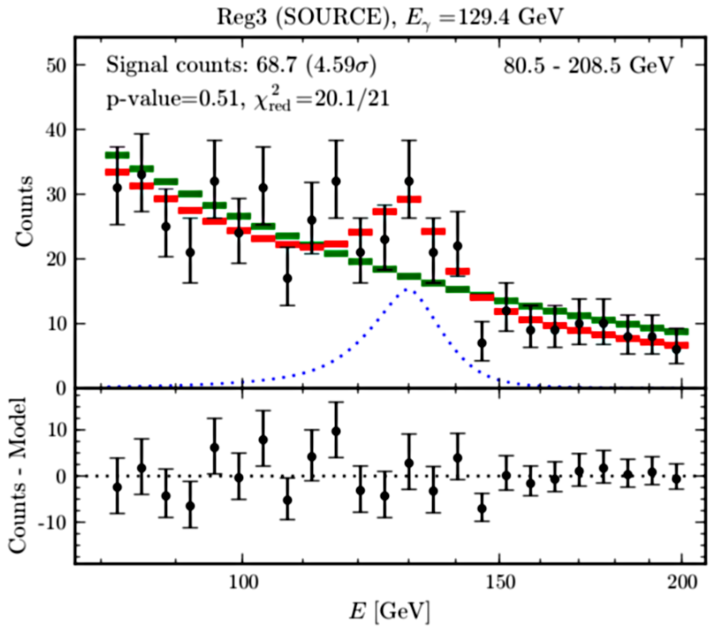

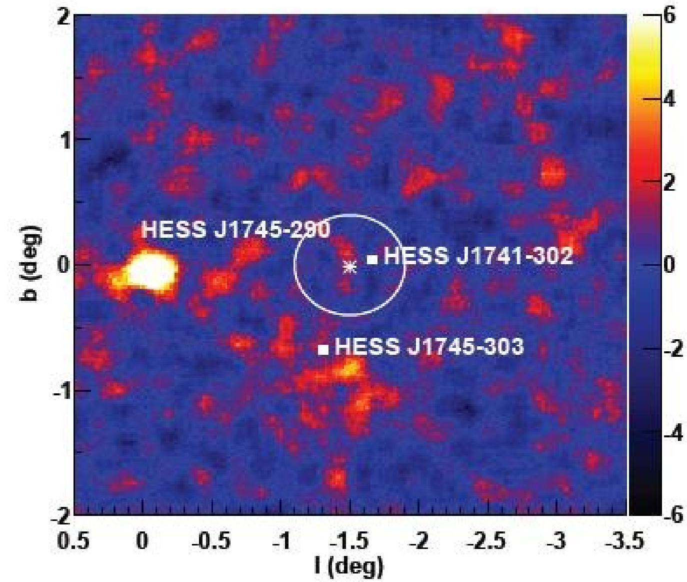

– an analysis of a 5-year data sample collected by Fermi-LAT in a sky region close to the Galactic Center resulted in a hint for a line-like signal at an energy of 130 GeV

– a new search for dark matter line-like signals in the vicinity of the Galactic Centre was performed with the complete HESS-II array

– no significant excess associated with dark matter annihilation was found in the energy range between 100 GeV and 2 TeV

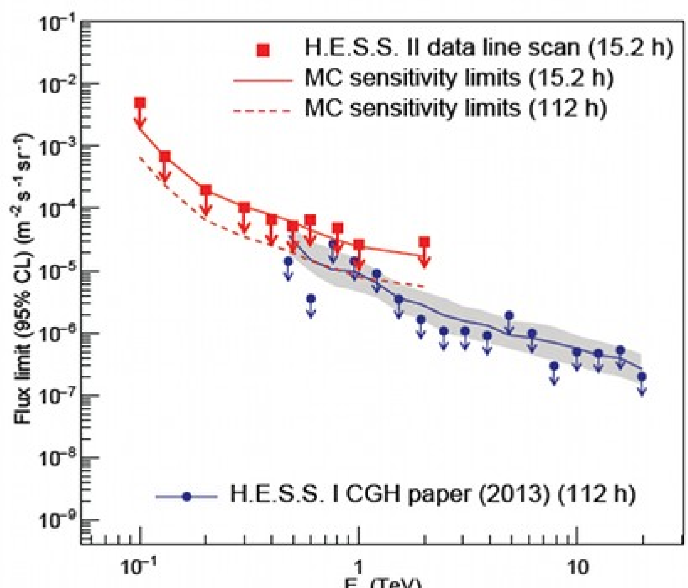

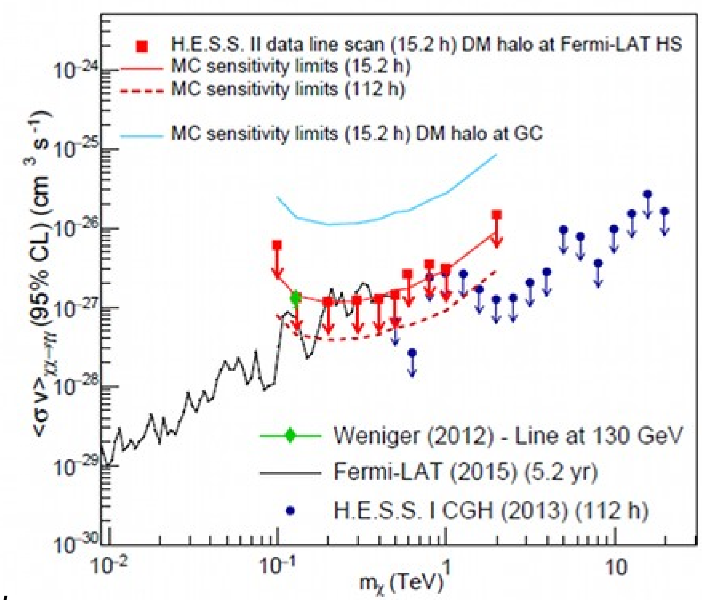

Cosmic ray electrons

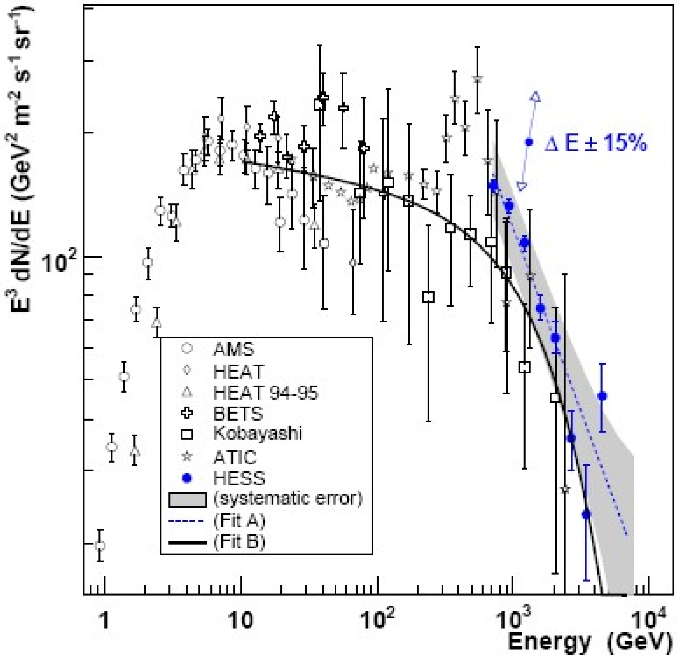

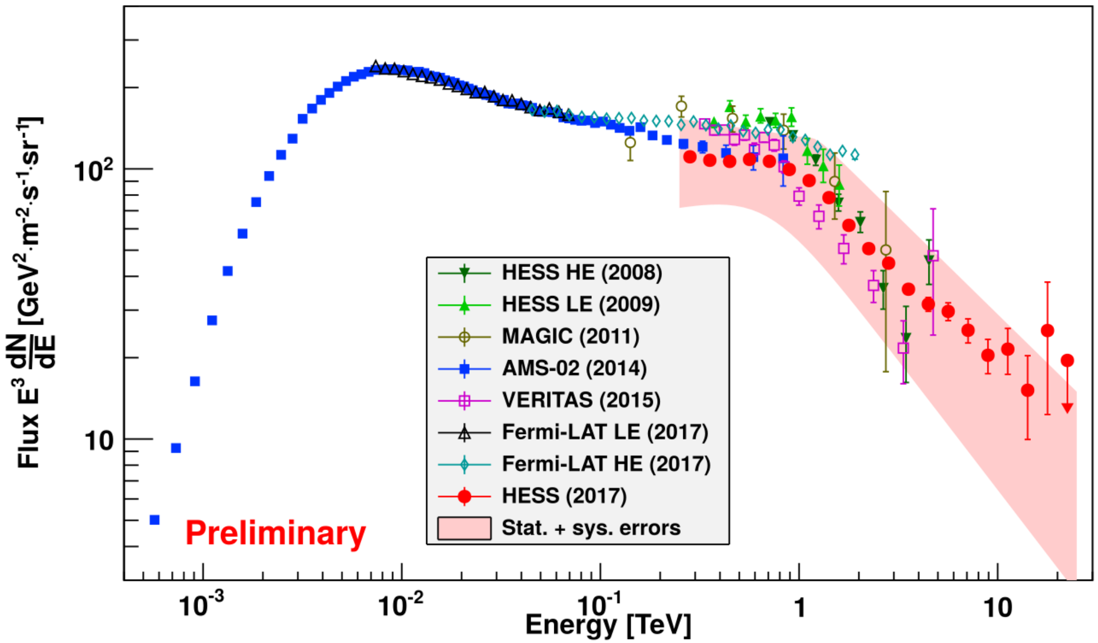

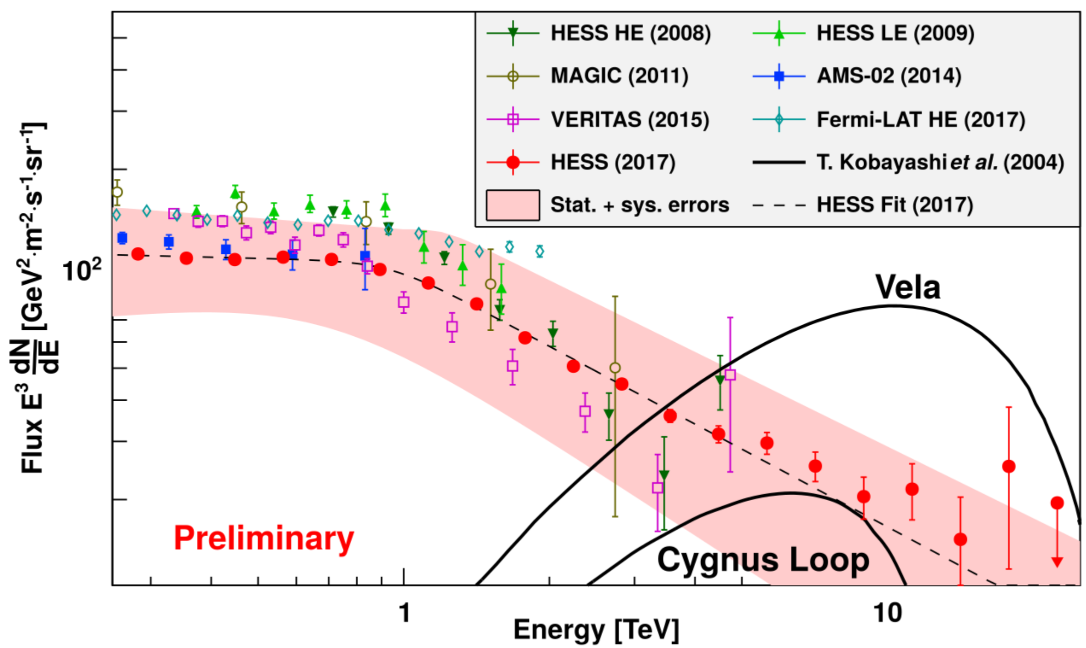

– first measurement of cosmic-ray electrons up to energies of ~ 20 TeV

– break in the spectrum - the transition between a regime where a large number of sources contribute to the spectrum, to a regime where only a few, the closest ones from Earth, are able to contribute

– some model of pulsar emission excluded by data

Extraterrestrial signal

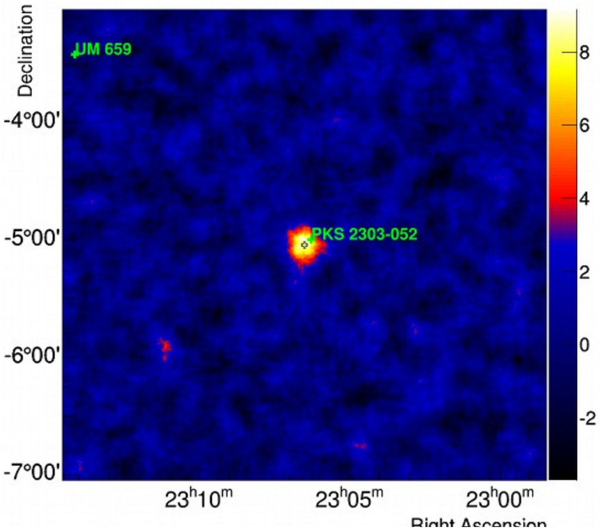

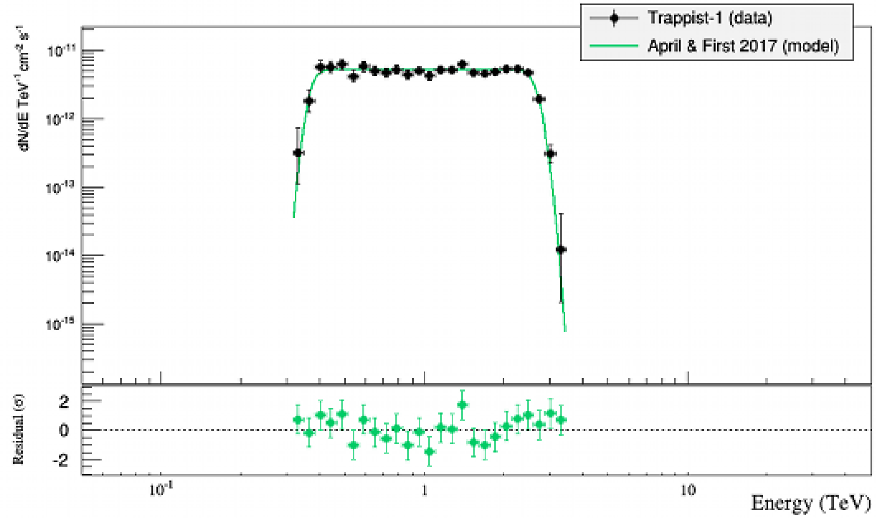

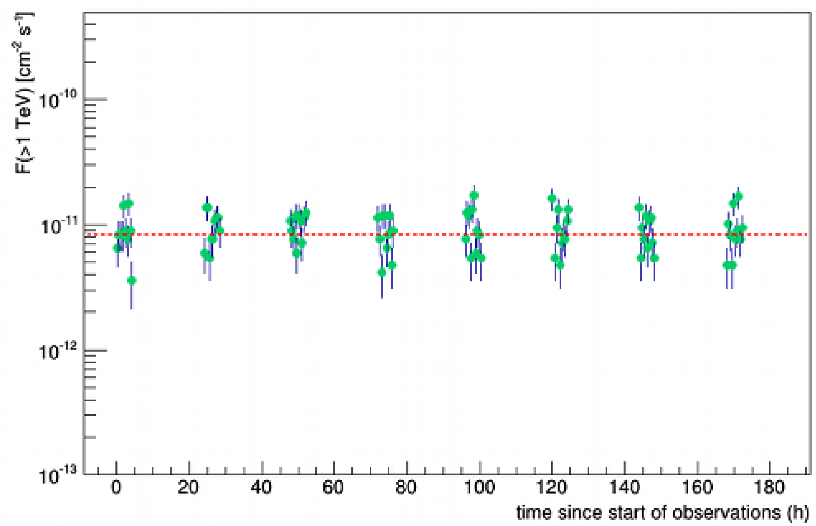

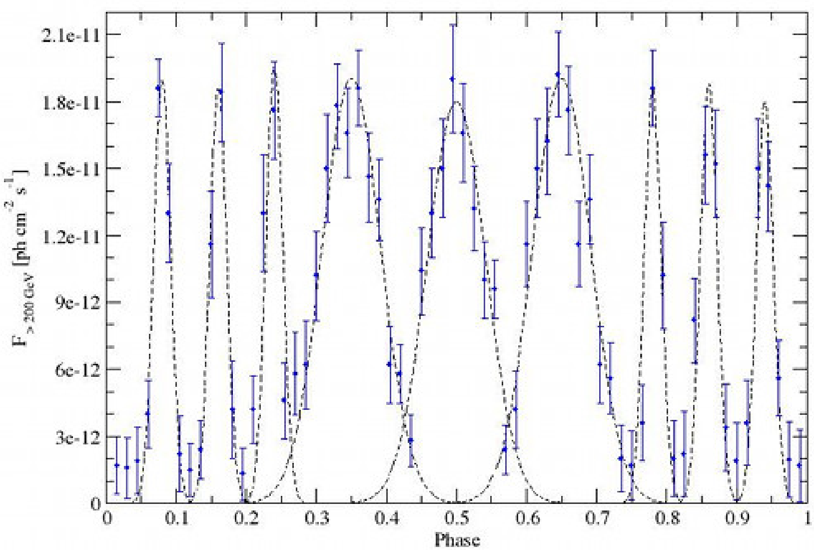

SUMMARY

– H.E.S.S. still performs very well in many aspects of astroparticle research

– addition of CT5 telescope, mirror recoating and camera upgrade allowed for further improvement in performance

– H.E.S.S. is still the only **hybrid system** – a pathfinder for the Cherenkov Telescope Array (CTA)

– the future of H.E.S.S. under discussion